Journal of the Geological Society, London, Vol. **164**, 2007, pp. 637–652. Printed in Great Britain.

An Oligocene extrusion wedge of blueschist-facies nappes on Evia, Aegean Sea, Greece: implications for the early exhumation of high-pressure rocks

UWE RING[1], JOHANNES GLODNY[2], THOMAS WILL[3] & STUART THOMSON[4]

[1]*Department of Geological Sciences, Canterbury University, Christchurch 8004, New Zealand (email: uwe.ring@canterbury.ac.nz)*

[2]*GeoForschungsZentrum Potsdam, 14473 Potsdam, Germany*

[3]*Institut für Mineralogie, Universität Würzburg, 97074 Würzburg, Germany*

[4]*Department of Geology and Geophysics, Yale University, New Haven, CT 06520, USA*

Abstract: We show that the Styra Nappe of the Cycladic Blueschist Unit on Evia constitutes a wedge of high-pressure rocks extruded during early stages of orogeny. The nappe pile on Evia was assembled during D_2 top-to-the-SSW-directed thrusting (in restored Oligocene coordinates), which emplaced the Styra and Ochi nappes of the Cycladic Blueschist Unit above the Almyropotamos Nappe between *c*. 33 and 21 Ma. Peak metamorphism of the Almyropotamos Nappe at *c*. 23 Ma occurred at lower metamorphic pressure, showing exhumation of the Styra Nappe during underthrusting and burial of the Almyropotamos Nappe. This exhumation was largely accomplished by the D_2 top-to-the-NNE-displacing Mt. Ochi normal-sense shear zone. Normal shearing commenced at *c*. 33 Ma under peak high-pressure metamorphism in the Styra and Ochi nappes. Fission-track dating indicates slow cooling after D_2 in the Styra Nappe. Subsequently, the former thrust contact between the Almyropotamos Nappe and the Styra Nappe was reactivated as a D_3 top-to-the-ESE extensional shear zone and this extensional phase led to the formation of a number of Middle to Late Miocene graben. Our main conclusion is that there is strong evidence for an Oligocene extrusion wedge accomplishing the early exhumation of the Styra Nappe, which demonstrates the importance of extrusion wedges for the initial exhumation of the Cycladic Blueschist Unit.

The central Hellenides in the Aegean region comprise the considerably exhumed Cycladic Blueschist Unit, which allows detailed studies of the relationship between subduction–underthrusting, high-pressure metamorphism and exhumation. The exhumation of the Cycladic Blueschist Unit has been widely attributed to extensional faulting along a few large-scale detachment faults (Lister *et al*. 1984). Several studies have shown that most of these detachments operated in the Middle to Late Miocene and accomplished only limited exhumation of the Cycladic Blueschist Unit (Avigad *et al*. 1997; Keay *et al*. 2001; Ring *et al*. 2003*a*; Kumerics *et al*. 2005; Brichau *et al*. 2006). However, geological constraints demand 30–40 km of exhumation of the Cycladic Blueschist Unit soon after its Eocene high-pressure metamorphism (Ring *et al*. 1999*a*; Gessner *et al*. 2001*a*), and Ring *et al*. (2007) showed that in the easternmost Aegean and adjacent western Turkey this early exhumation was accomplished by an Eocene extrusion wedge, the latter being defined by a thrust at its base and a normal fault at its top. Because the basal thrust and the normal fault at the top operate in concert with each other during overall horizontal shortening, considerable tectonic exhumation of the extruding wedge did not cause significant attenuation of the crust (Ring *et al*. 1999*b*, 2007). It should be noted that the term 'normal fault' relates only to the relative sense of shear along a shear zone or fault, which may be due to overall shortening or extension, whereas 'extensional fault' implies that a shear zone or fault resulted from overall horizontal extension.

A critical question is whether there is also evidence for an extrusion wedge exhuming the Cycladic Blueschist Unit in other parts of the Aegean, because this would strongly imply that extrusion wedges played the key role in the early exhumation of the Cycladic Blueschist Unit. On the island of Evia in the western Aegean Sea, blueschist-facies structures are well preserved. Thus, the aim of this study was to test whether there is evidence for an extrusion wedge aiding the early exhumation of the Cycladic Blueschist Unit on Evia through an investigation of the interplay between crustal shortening, high-pressure metamorphism and normal faulting.

Structures related to early crustal shortening and the development of high-pressure metamorphism have rarely been documented in the Aegean (Vandenberg & Lister 1996; Ring *et al*. 1999*c*, 2007; Shaked *et al*. 2000), because they were strongly overprinted by later extensional deformation. By far most of the horizontal extension and attenuation of the crust occurred since the Miocene, leading to the formation of the Aegean Sea basin, with the thinnest part of the Aegean crust ($<$19 km) occurring south of Evia (Tsokas & Hansen 1997; Fig. 1, insert).

Herein we argue that on Evia thrusting of the passive-margin sequence of the Cycladic Blueschist Unit (Styra Nappe) onto the Basal Unit (Almyropotamos Nappe) was coeval with crustal-scale normal faulting between the Styra Nappe and the overlying ophiolitic mélange (Ochi Nappe) resulting in an extrusion wedge of Oligocene age. Together with the recently reported work by Ring *et al*. (2007) on the easternmost Aegean and western Turkey, this finding suggests that extrusion wedge formation is important for the exhumation of the Cycladic Blueschist Unit and possibly also for high-pressure rocks in other orogens. We further argue that on Evia normal faulting subsequently progressed structurally downward, resulting in a number of Neogene extensional basins along the former thrust contact between the Styra and Almyropotamos nappes.

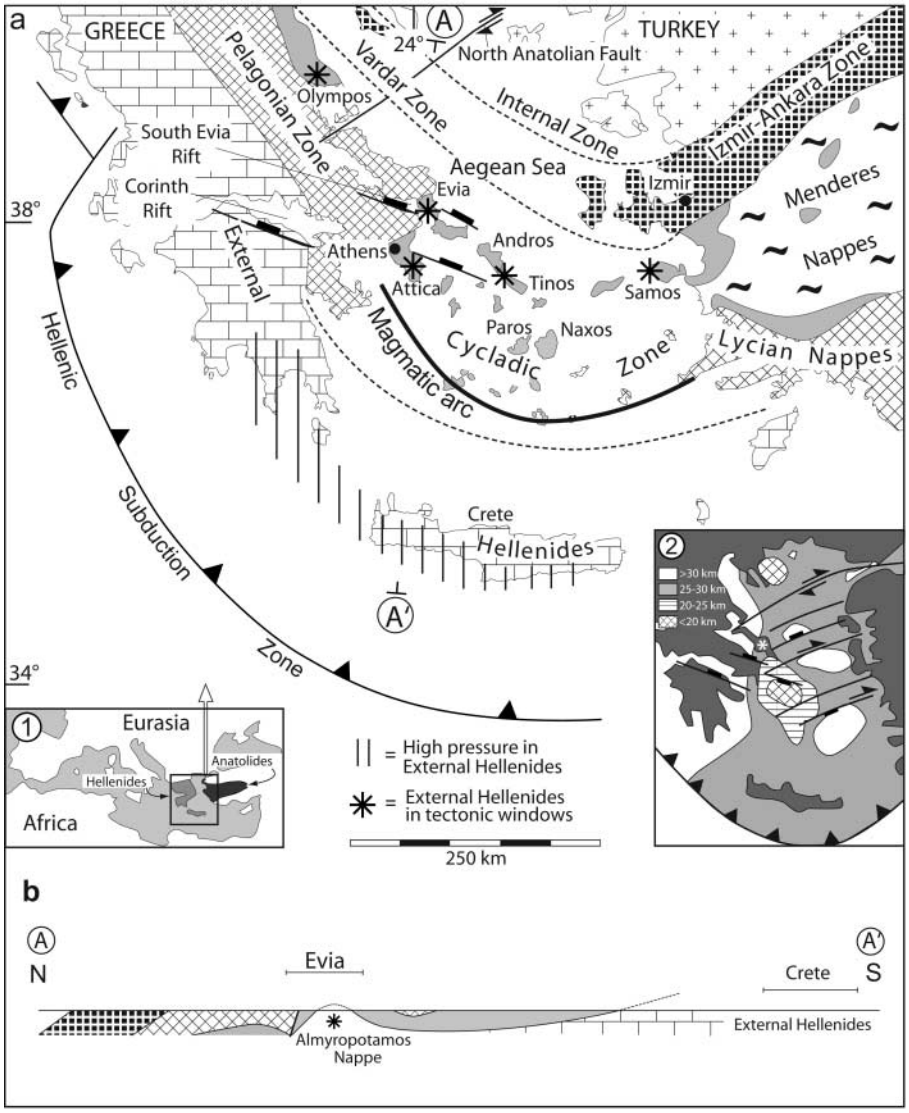

Fig. 1. (**a**) Generalized tectonic map of the Aegean region showing major tectonic units and present-day position of the Hellenic subduction zone. The Cycladic Blueschist Unit is the dominant tectonic unit of the Cycladic zone in the central Aegean and is overlain by the continental Pelagonian zone–Lycian nappes and oceanic Vardar–Izmir–Ankara Zone. The Basal Unit of the Cyclades is part of the External Hellenides and crops out below the Cycladic Blueschist Unit in some windows (asterisks show Olympos and Attica windows on the Greek mainland, Almyropotamos and Panormos windows on Evia and Tinos, and Kerketas Nappe on Samos). The Cycladic Blueschist Unit and Vardar–Izmir–Ankara Zone form high-pressure belts of Cretaceous to Early Tertiary age that span a wide area from the Greek mainland across the northern Aegean Sea into Turkey. Early Miocene high-pressure rocks of the External Hellenides (vertically ruled pattern) occupy a more restricted area than older high-pressure rocks and occur in the Basal Unit in the Cyclades and south or SE of the Late Pliocene to Recent volcanic arc delineated by calc-alkaline volcanoes. Box indicates location of the map shown in Figure 2. Insets: (1) Mediterranean region and location of main map; (2) crustal thicknesses in the Aegean region after Tsokas & Hansen (1997) and network of NE–SW-trending dextral oblique-slip faults and WNW–ESE-trending normal faults after Kiratzi & Louvari (2003) (note that thin crust south of Evia is associated with these two sets of neotectonic faults). (**b**) NNE–SSW cross-section of the nappe pile in the western Aegean.

Setting

Previous research has outlined several tectonic zones in the Hellenide–Anatolide orogen in the eastern Mediterranean (Fig. 1). The tectonic zones are distinguished by rock type, stratigraphy, tectonometamorphic history and pre-orogenic palaeogeography (Dürr *et al*. 1978; Robertson *et al*. 1991). The Hellenides in the Aegean region can be subdivided from top (internides) to bottom (externides) into (1) the Internal Zone, (2) the Vardar–Izmir–Ankara Zone, (3) the Pelagonian Zone, (4) the Cycladic Zone, and (5) the External Hellenides.

The Internal Zone is considered part of Eurasia underneath which oceanic crust of Neotethys was subducted. The related suture is the ophiolitic Vardar–Izmir–Ankara Zone. The Pelagonian Zone is a thick-skinned thrust belt that crops out below the Vardar–Izmir–Ankara Zone. The Pelagonian Zone is underlain by the Cycladic Zone, which is dominantly made up of the Cycladic Blueschist Unit. The Cycladic Blueschist Unit is overlain on some Aegean islands (e.g. Samos, Tinos, Andros; Fig. 1) by the so-called Upper Unit. The Upper Unit is a non- to weakly metamorphosed nappe that is overlain by Miocene or Pliocene sediments.

From top to bottom the Cycladic Blueschist Unit comprises three composite nappes: (1) an ophiolitic mélange; (2) a Carboniferous–Permian to latest Cretaceous passive-margin sequence; (3) a Carboniferous basement (Ring *et al*. 1999*c*). As a result of intense deformation related to nappe stacking and subsequent extensional reactivation subparallel to the earlier thrust planes, slices of these composite nappes may occur in adjacent nappes. The Basal Unit as part of the External Hellenides (Godfriaux 1968) occurs below the Cycladic Blueschist Unit and is exposed in the Mt. Olympos window, on the Attica peninsula, as well as on Evia, Tinos and Samos (Fig. 1).

The Hellenide–Anatolide orogen has some along-strike differences in orogenic architecture (Ring *et al*. 1999*a*; Gessner *et al*. 2001*a*). The major dissimilarity between the Hellenides and the Anatolides of western Turkey is the palaeogeographical origin of the lowermost exposed unit in the two orogens. In the east the Menderes Nappes are part of the Anatolian microplate, whereas in the west the External Hellenides belong to the Adriatic microplate (Gessner *et al*. 2001*b*, 2004). Anatolia collided with Eurasia in the Eocene in western Turkey and the easternmost Aegean; in contrast, deep underthrusting

of the Basal Unit (External Hellenides), as part of Adria, did not start before the Oligocene at *c*. 35 Ma in the western Aegean (Thomson *et al*. 1998; Ring & Layer 2003; van Hinsbergen *et al*. 2005*a*).

Geology of southern Evia

In this study we concentrate on the nappe pile of southern Evia (Fig. 2). In the northernmost part of the study area, the uppermost tectonic unit, the Pelagonian Zone, is exposed. It consists of Palaeozoic schist overlain by Triassic–Jurassic marble (Jacobshagen 1986; Katsikatsos 1991). West of Kimi, this sequence is transgressively overlain by Late Cretaceous limestone and Palaeocene to Early Eocene flysch (Dubois & Bignot 1979; Xypolias *et al*. 2003). The tectonic unit below the Pelagonian Zone is the Ochi Nappe, which represents the ophiolitic mélange of the uppermost Cycladic Blueschist Unit. The Ochi Nappe contains blocks of metagabbro, metawehrlite and metabasalt in a serpentinitic matrix as well as metarhyolite, piemontite-rich chert, quartzite and carbonate-rich schist (Jacobshagen 1986; Katsikatsos 1991; Katzir *et al*. 2000). The underlying Styra Nappe represents the passive-margin sequence of the Cycladic Blueschist Unit and consists of a thick (*c*. 1000 m) succession of metabauxite-bearing marble, quartzite and metapelite, as well as metabasite and serpentinite lenses at its base. The underlying Almyropotamos Nappe belongs to the Basal Unit. It is mainly composed of a thick (*c*. 2000 m) succession of Triassic to Middle Eocene marble with thin metapelite intercalations. Above the marble occurs a *c*. 1500 m thick Late Eocene to Oligocene metaflysch that contains abundant olistoliths (Dubois & Bignot 1979).

The metamorphic sequence is overlain by Neogene sediments. The largest Neogene basin is the Kimi Basin, which is made up of a lower sequence of up to 500 m thick alluvial fan deposits, and fluvial to lacustrine sediments of Burdigalian age (i.e. *c*. 21–16 Ma) (Katsikatsos *et al*. 1981; H. de Bruijn, pers. comm.). Sediment thickness and grain size of the lower sequence increase markedly to the west (Xypolias *et al*. 2003). The upper sequence is *c*. 800 m thick and consists entirely of alluvial fan deposits and conglomerates of Late Miocene age (Katsikatsos *et al*. 1981; Kokkalas 2001). The 15–13 Ma Oxylithos sub-volcanic complex in the central basin consists of dacite and andesite (Pe-Piper & Piper 1994) and is regarded as part of the magmatic arc of the southward retreating Hellenic subduction zone. To the south of the Kimi Basin there are a few small Neogene basins that are largely confined to the tectonic contact between the Styra and Almyropotamos nappes. They contain conglomerate, sandstone and marl with numerous intercalations of travertine limestone. The deposits contain the Pikermian vertebrate fauna, which places them in the Middle to Late Miocene (Katsikatsos 1991). A Quaternary basin occurs around Karystos on the southern coast of Evia.

Previous work

Jacobshagen (1986) and Katsikatsos (1991) described the general structure and lithology of southern Evia. Shaked *et al*. (2000) and Xypolias *et al*. (2003) showed that the Styra Nappe was thrust over the Almyropotamos Nappe along the Evia thrust (*sensu* Xypolias *et al*. 2003). However, based on fold vergence, Shaked *et al*. (2000) envisaged top-to-the-south thrusting, whereas Xypolias *et al*. (2003) mapped ENE–WSW-trending stretching lineations (as did Gautier & Brun 1994) and top-to-the-ENE shear-sense indicators at the Evia thrust. Maluski *et al*. (1981) and Ring & Layer (2003) argued that ^{40}Ar–^{39}Ar white mica ages of *c*. 35–30 Ma from mylonites date initial thrusting under high-pressure conditions of the Styra Nappe onto the Almyropotamos Nappe. Kokkalas (2001) and Xypolias *et al*. (2003) studied the contacts between the Pelagonian Zone, the Cycladic Blueschist Unit, the Almyropotamos Nappe and the Kimi Basin near Alivieri and showed that the lower sequence of the Kimi Basin was internally imbricated and overthrust by the Pelagonian Zone during NE–SW shortening in the Early Miocene. This event created the Kimi thrust (*sensu* Xypolias *et al*. 2003) (Fig. 2). Subsequently, the Kimi Basin was subjected to two phases of extensional deformation, the earlier one related to ENE–WSW extension and the final one related to NNE–SSW extension.

Based on the rare presence of glaucophane-bearing rocks in the Almyropotamos Nappe, Shaked *et al*. (2000) estimated metamorphic pressures of *c*. 8–10 kbar for temperatures of *c*. 350 °C. Ring & Reischmann (2002) dated this high-pressure metamorphism at *c*. 23 Ma. This early Miocene age is similar to that of other exposures of high-pressure rocks in the Basal Unit in the Aegean (Ring *et al*. 2001). Simple calculations using the *P*–*T* estimates for the Almyropotamos Nappe, an Oligocene subduction rate of 25–30 km Ma^{-1} (Ring *et al*. 1999*a*) and a 10–15° dip of subduction (Giunchi *et al*. 1996) show that underthrusting of the Almyropotamos Nappe to its depth of high-pressure metamorphism took at least *c*. 5–9 Ma, which is about the time span between initial thrusting of the Styra Nappe onto the Almyropotamos Nappe at *c*. 35–30 Ma and high-pressure metamorphism in the latter at *c*. 23 Ma. The Late Eocene to Oligocene depositional age of the Almyropotamos metaflysch, which subsequently underwent high-pressure metamorphism (Shaked *et al*. 2000), fits into this age pattern.

Using the observed mineral assemblage epidote–sodic amphibole–omphacitic clinopyroxene, together with the petrogenetic grid of Evans (1990), and oxygen isotope data, Katzir *et al*. (2000) and Shaked *et al*. (2000) estimated *P*–*T* conditions of >10–12 kbar and 400–450 °C for metagabbro from the Ochi Nappe. Age data from other Aegean islands suggest that the peak of high-pressure metamorphism occurred at 55–45 Ma (Wijbrans *et al*. 1990; Ring & Layer 2003; Tomaschek *et al*. 2003). Katzir *et al*. (2000) showed that the metabasic rocks of the Ochi Nappe re-equilibrated during decompression at <8 kbar and <350 °C. It should be noted that the *P*–*T* conditions for decompression in the Ochi Nappe are similar to the peak high-pressure *P*–*T* conditions reported for the Almyropotamos Nappe by Shaked *et al*. (2000).

van Hinsbergen *et al*. (2005*b*) recently revised the timing and magnitude of Neogene rotations in the western Aegean. They concluded that western Greece, including Evia (Kissel *et al*. 1986; Morris 1995), rotated *c*. 40° clockwise between *c*. 14 and 8 Ma, followed by an additional 10° of clockwise rotation after 4 Ma.

Architecture of southern Evia

The general architecture of southern Evia is controlled by the window of the Almyropotamos Nappe and the associated Evia thrust (Figs 2 and 3). Within the Almyropotamos Nappe there is the Almyropotamos thrust (*sensu* Xypolias *et al*. 2003), which brings Triassic to Early Cretaceous marble on top of Late Cretaceous to Middle Eocene marble. A number of post-thrust Neogene basins occur along the Evia thrust. Towards the SE the nappe pile is moderately dipping away from the Almyropotamos window. West of Mt. Ochi, the NW-dipping Karystos normal

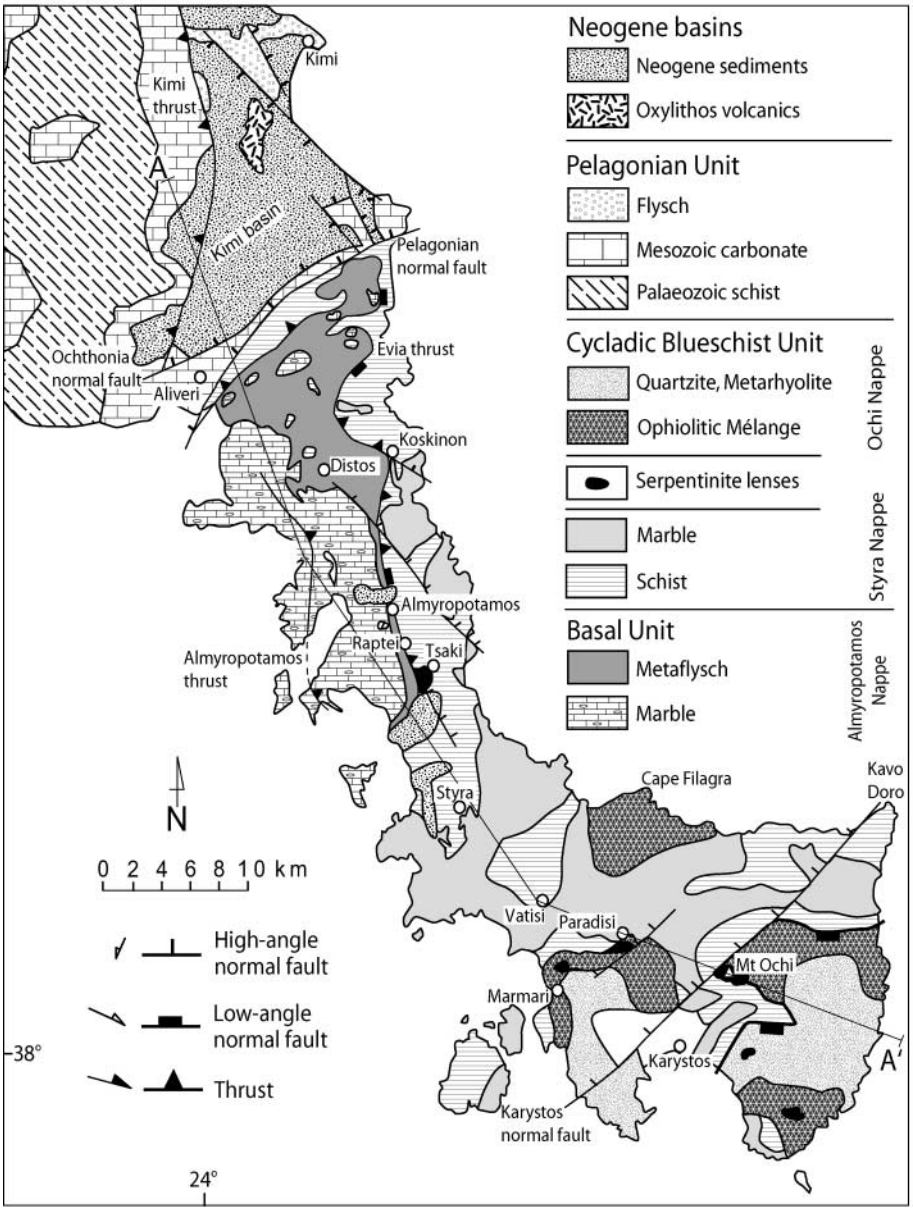

Fig. 2. Tectonic map of southern Evia showing major structures and tectonic contacts between units (after Jacobshagen 1986; Katzir *et al*. 2000; Xypolias *et al*. 2003) (note numerous marble olistoliths in the Almyropotamos metaflysch).

fault brings up the Mt. Ochi normal shear zone in its footwall. To the NW of the Almyropotamos window, the tectonic relationships are more complicated. In general, the rocks are more steeply dipping than in the south and the steep dips are caused by the Pelagonian and Ochthonia normal faults, both of which also have a dextral strike-slip component (Kokkalas 2001). The Pelagonian normal fault basically brought down the Pelagonian Zone and placed it in close proximity to the Almyropotamos Nappe, thereby juxtaposing the highest with the lowest tectonic units of the nappe pile. The Ochthonia normal fault marks the southern boundary of the Kimi Basin. The lower sequence of the Kimi Basin onlaps the Pelagonian Zone in the west and is imbricated, with the Kimi thrust being the major shortening structure (Xypolias *et al*. 2003).

Petrography

The rocks of the Ochi and Styra nappes were metamorphosed at greenschist- to blueschist-facies conditions and are invariably very fine grained. Mafic rocks can be unfoliated, strongly foliated or mylonitized. Minerals found in these rocks include sodic amphibole, epidote, albite, white mica, opaque minerals and, locally, quartz. Retrograde green and colourless calcic amphibole and chlorite can occur. Relict magmatic diopsidic clinopyroxene is present in a few samples. The mineral assemblage sodic amphibole–epidote–white mica is ascribed to blueschist-facies conditions and the assemblage calcic/barroisitic amphibole–epidote–chlorite–albite to a subsequent decompression stage under transitional blueschist- to greenschist-facies conditions. Some samples are strongly mylonitized, with the entire blueschist-facies mineral assemblage being strongly aligned in the foliation plane. Sodic amphibole in these samples is always acicular with a very high aspect ratio. These blueschist-facies mylonites were found at Cape Filagra and at Mt. Ochi.

Metapelitic rocks preserving evidence for high-pressure metamorphism were not found; instead, mineral assemblages including white mica, quartz, albite, opaque phases and minor chlorite and/or calcite testify to greenschist-facies conditions.

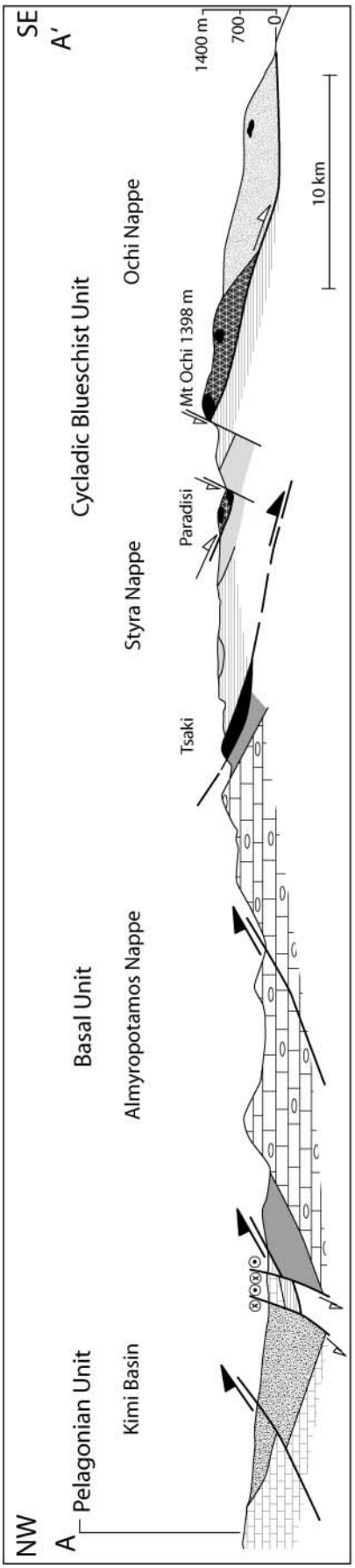

Fig. 3. NW–SE cross-section through the nappe pile of southern Evia, after Jacobshagen (1986), Katzir *et al.* (2000) and Xypolias *et al.* (2003). It should be noted that the cross-section is at a high angle to tectonic transport during D_2 and D_3, and that D_2 top-to-the-ENE shearing affected the upper Styra Nappe and entire Ochi Nappe pervasively.

Commonly, the greenschist-facies metasedimentary schists are strongly foliated. Unfortunately, the extremely fine-grained nature of the samples prevented successful mineral analyses and quantification of P–T conditions.

Structures and their relation to metamorphism

Early structures

Relics of early D_1 structures are a locally penetrative S_1 foliation associated with isoclinal intra-folial folds (Fig. 4). Xypolias *et al*. (2003) described two generations of these early intra-folial folds. At the beach near Cape Filagra (Fig. 2), S_1 is the main fabric in outcrops (Fig. 4a). It is associated with a WSW–ENE-trending stretching lineation, STR_1, which is mainly composed of extremely acicular glaucophane. S_1 in the blueschists is made up of glaucophane, epidote, phengitic white mica, albite and quartz, which formed under high-pressure epidote–blueschist-facies metamorphism. S_1 and STR_1 are folded about F_2 folds, which have axes parallel to STR_1. Refolding caused a locally pervasive D_1–D_2 transposition.

Interlayered D_1 blueschist- and D_2 greenschist-facies rocks are another example of D_1–D_2 transposition at Cape Filagra. These extremely fine-grained rocks consist of fresh blueschist-facies D_1 mylonites that are intimately associated with retrogressed greenschist-facies mylonites. The latter have a pervasive foliation that is made up of acicular calcic amphibole, albite, minor white mica and secondary chlorite. A few relict glaucophane grains, which are invariably rimmed by calcic amphibole, are preserved in the foliation and testify to former blueschist-facies conditions of the greenschist-facies rocks. The blueschist- and greenschist-facies structures are always parallel to each other.

Fig. 4. Early structures. (**a**) Early S_1 foliation folded and crenulated by west-dipping S_2 in metabasic rocks; beach at Cape Filagra (38°09′26″N, 24°23′51″E). (**b**) Top-to-the-ENE shear bands reworking earlier D_1 fabric in quartzite at Mt. Ochi (38°03′36″N, 24°27′57″E); isoclinal D_1 intra-folial folds delineated by milky quartz layers are preserved in microlithons between D_2 shear bands. (**c**) Folded D_1 fabric deformed by top-to-the-ENE-displacing shear zone in quartzite at Mt. Ochi (38°03′01″N, 24°27′53″E).

Main deformation event

The main-phase D_2 structures developed under peak high-pressure metamorphism and the subsequent transitional blueschist- to greenschist-facies overprint. In southeasternmost Evia near Kavo Doro, the structures show a progressive development through sub-greenschist-facies and brittle conditions (Fig. 5). The penetrative S_2 foliation is the regional foliation (Fig. 6a). S_2 is associated with a pervasive, subhorizontal, ENE–WSW-trending stretching lineation, STR_2, expressed by stretched quartz–albite aggregates and oriented mineral growth (Fig. 5a). Shear-sense indicators associated with STR_2 show a progressive change from top-to-the-WSW in the structurally deep levels to top-to-the-ENE in the high levels of the nappe pile (Fig. 7).

Shear bands at the Almyropotamos and Evia thrusts yielded a consistent top-to-the-WSW sense of shear. Serpentinite just above the Evia thrust west of Tsaki exhibits S–C and shear-band structures indicative of top-to-the-WSW shear associated with S_2 (Fig. 5b). X-ray diffraction analysis shows that antigorite is the stable serpentine mineral in these structures, indicating that they formed above *c*. 400 °C. Marble and metapelite east of Tsaki also show well-developed top-to-the-WSW shear bands and S–C structures associated with S_2. Metabasic lenses in the basal Styra Nappe show top-to-the-WSW S–C structures as well. In the metabasic rocks, STR_2 is made up by aligned and stretched phengite, glaucophane, actinolite, epidote, chlorite and quartz. The S–C structures are characterized by white mica, epidote, albite, chlorite and quartz assemblages, most of which grew during retrogression of high-pressure glaucophane-bearing parageneses (note that sample EV05-25a from this outcrop was used for Rb–Sr dating and is described in detail below). In metapelite lenses along the Almyropotamos thrust we mapped shear bands yielding a top-to-the-WSW sense of shear (Fig. 7). In all samples investigated, the orientation of the retrograde minerals is strictly parallel to the peak high-pressure minerals.

Near Styra and just to the south of it, the huge marble sequence shows two generations of spectacular isoclinal folds with axes parallel to STR_2. The kinematic indicators yielded a consistent top-to-the-WSW shear sense in upright and overturned fold limbs, indicating that the two fold generations are synchronous with STR_2.

Further south, between Styra and Vatisi, the kinematic indicators begin to show an alternating top-to-the-WSW and top-to-the-

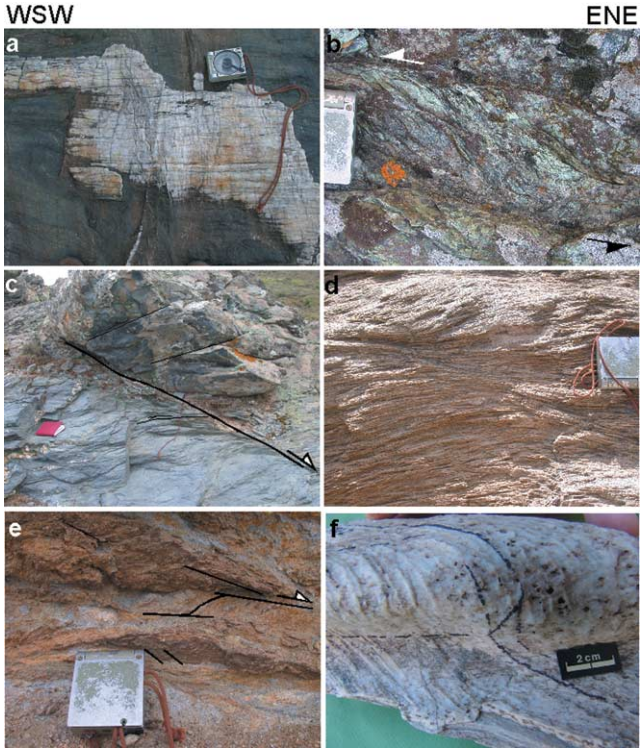

Fig. 5. Main deformation structures. (**a**) Penetrative stretching lineation associated with main foliation; beach north of Gianitisi (38°09′26″N, 24°23′51″E). (**b**) S–C structures indicating top-to-the-WSW shear in serpentinite at base of the Styra Nappe at Tsaki (38°14′14″N, 24°13′12″E). (**c**) Top-to-the-ENE-displacing shear bands and low-angle normal fault in blueschist on the southern slopes of Mt. Ochi (38°01′43″N, 24°27′58″E); in glaucophane schist in the lower half of the photograph shear bands are subhorizontal and shearing commenced under blueschist-facies conditions; a low-angle normal fault juxtaposes a massive glaucophane block in the hanging wall with foliated blueschist in the footwall, and structures in the fault are characterized by greenschist- to sub-greenschist-facies mineral assemblages. (**d**) Greenschist-facies top-to-the-ENE shear bands in metapelite SE of Karystos (37°57′49″N, 24°28′30″E). (**e**) Brittle top-to-the-ENE shear bands associated with gouge zones at Kavo Doro (38°08′02″N, 24°34′09″E). (**f**) Late D_2 isoclinal fold refolding STR_2 slightly about north–south-trending axes; sense of asymmetry of the fold is consistent with top-to-the-east shear (38°03′01″N, 24°27′53″E).

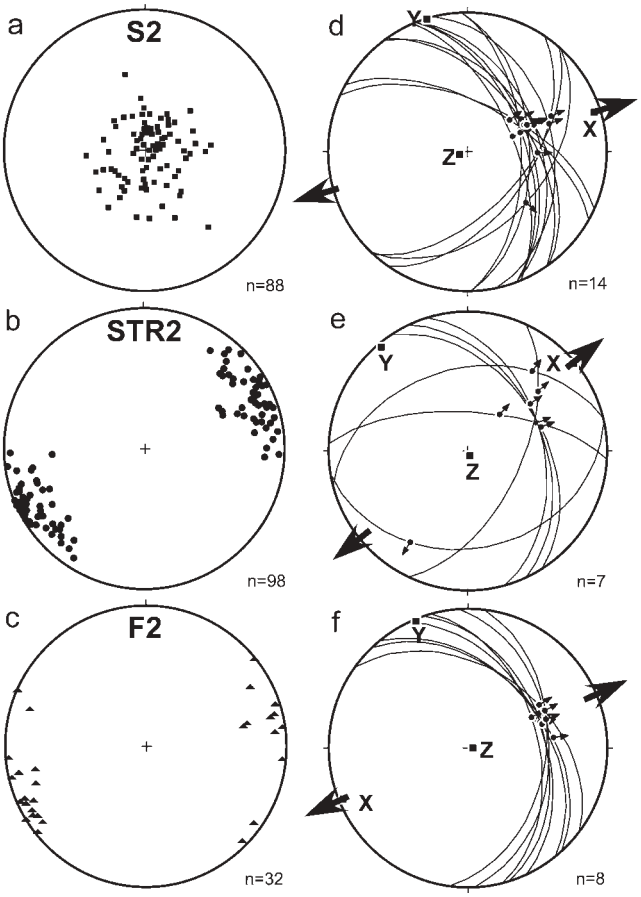

Fig. 6. Stereographic, lower-hemisphere projections of (**a**) S_2, (**b**) STR_2 and (**c**) F_2. (**d**–**f**) D_2 fault-slip analysis in moderately to steeply dipping D_2 normal faults; data from Cape Filagra (**d**, **e**) and Kavo Doro (**f**); localities where fault-slip data were obtained are shown in Figure 7.

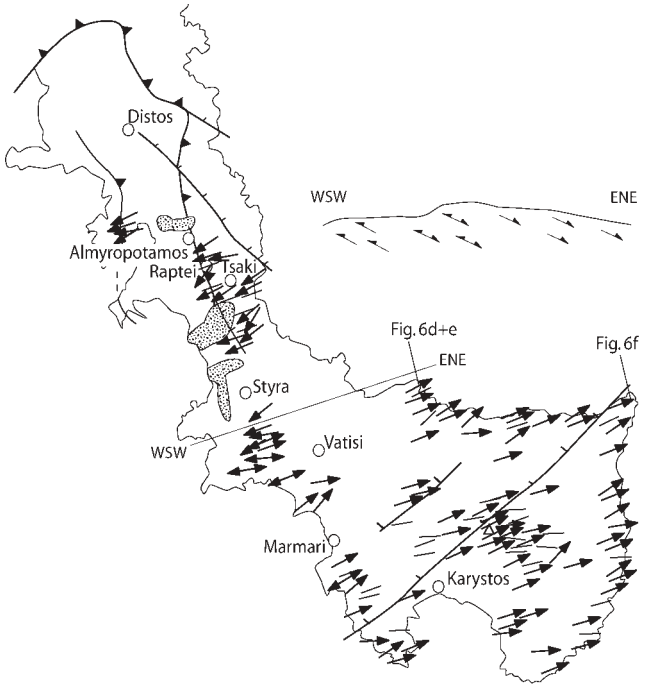

Fig. 7. Map and schematic cross-section showing STR_2; arrowheads indicate the hanging-wall sense of shear associated with STR_2. It should be noted that the shear sense is top-to-the-WSW in the lower parts of the nappe pile in the northern half of the study area, is alternating top-to-the-WSW and top-to-the-ESE in the central part between Styra and Vatisi, and pervasively top-to-the-ESE in the upper structural levels in SE Evia. Also, the region of pronounced brittle deformation at the coastline north of Mt. Ochi should be noted.

ESE shear sense associated with S_2 and STR_2 (Fig. 7). Some outcrops in layered marble show a consistent top-to-the-WSW sense of shear, whereas outcrops a few metres away show a uniform top-to-the-ENE shear sense and other outcrops are characterized by alternating shear senses. In all cases isoclinal folds with axes parallel to STR_2 occur and the alternating shear senses are not caused by inversion owing to later folding.

In regions where the ophiolitic mélange of the Ochi Nappe crops out in southeastern Evia, the kinematic indicators associated with S_2 yielded a consistent top-to-the-ENE sense of shear (Figs 5c-e and 7). Impure marble on the eastern slopes of Mt. Ochi shows spectacular isoclinal folds with axes parallel to STR_2. The kinematic indicators yielded a uniform top-to-the-ENE shear sense in upright and overturned fold limbs, indicating that the isoclinal folds are synchronous with STR_2. A subsequent fold generation refolded STR_2 about northerly trending axes (Fig. 5f). Folds of this generation are distinctly asymmetric and a modest reorientation of STR_2 and the associated shear sense occurs only in the short limbs of the folds. The sense of asymmetry of these folds is consistent with top-to-the-ENE shear.

At Mt. Ochi, a D_2 top-to-the-ENE shear zone that is several hundreds of metres thick is exposed in metabasite and quartzite of the Ochi Nappe. The quartzite shows abundant shear zones (Fig. 4b and c) and isoclinal folds associated with D_2. Here, S_2 and STR_2 are made up by stretched quartz–albite–phengite aggregates in quartzite, and aligned phengite, glaucophane, actinolite, epidote and chlorite in metabasic rocks. In quartzitic glaucophane schist *c.* 500 m east of Mt. Ochi, S_2 developed in the stability field of a glaucophane–epidote–phengite–rutile assemblage. Glaucophane needles are perfectly aligned in S_2; the needles grew and were aligned parallel to STR_2. A well-developed top-to-the-ENE sense of shear is recorded by rotated albite and shear bands in which glaucophane and very small, recrystallized phengite grew. Retrograde chlorite locally overgrew S_2 but is still entirely aligned parallel to S_2 and STR_2.

In glaucophane schist on the southern slopes of Mt. Ochi, D_2 subhorizontal shear bands developed during blueschist-facies conditions (Fig. 5c). The subhorizontal shear bands become progressively steeper and grade into normal faults, which formed during sub-greenschist-facies retrogression of blueschist-facies assemblages (Fig. 5c). In the normal faults quartz is cataclastically deformed in certain zones and white mica and chlorite are kinked. To the north and (south)east of Mt. Ochi, subhorizontal D_2 structures with well-developed top-to-the-ENE shear bands (Fig. 5d) and asymmetric foliation boudinage formed during greenschist-facies conditions.

In general, S_2, STR_2 and the kinematic indicators formed during the peak of blueschist-facies conditions, which had already caused mineral growth during D_1. All glaucophane in the mylonites is acicular with an extremely high aspect ratio. If there was pre-S_1/S_2 amphibole growth we would expect a greater variety of crystal shapes. However, the structures continued to evolve during retrogression, as indicated by retrograde chlorite, partially mimetically overgrowing the high-pressure foliation, but commonly growing exactly parallel to it and STR_2. We envisage that the retrograde mineral growth occurred at P–T conditions of <8 kbar and <350 °C as inferred by Katzir *et al*. (2000) for similar assemblages. Quantitative P–T estimates failed because of analytical problems with the extremely fine-grained minerals and, especially, because of the lack of low-variance mineral assemblages in the samples.

At Kavo Doro, impressive cataclasites are exposed (Fig. 5e). Quartz, chlorite and mica in the metapelitic rocks are extensively cataclastically reworked, and there is abundant evidence for oxidizing, iron-rich aqueous solutions percolating through the rocks. The shear sense, as deduced mainly from Riedel structures in the subhorizontal cataclasite and gouge zones, is also consistently top-to-the-ENE. Deformation becomes markedly more brittle towards the ENE (Fig. 7). In general, the subhorizontal structures are cut by or grade into moderately to steeply dipping normal faults. Fault-slip data from the Kavo Doro and Cape Filagra areas yielded an ENE–WSW- to NE–SW-oriented extension direction (Fig. 6d–f).

Late extension

The last set of subhorizontal structures, D_3, mainly developed in the vicinity of the Evia thrust and includes greenschist- to sub-greenschist-facies top-to-the-ENE shear bands, which progressively evolved into normal faults (Figs 8 and 9). A new S_3 foliation developed in fold hinges of F_3 folds; elsewhere D_3 structures commonly used the older S_2 planes (Fig. 8a). S_3 contains a locally pervasive stretching lineation STR_3 (Fig. 8b), mainly expressed by elongated quartz–albite aggregates and alignment of chlorite and white mica. In zones of pervasive STR_3, isoclinal to tight F_3 folds are commonly parallel to STR_3 (Fig. 8c).

In the Almypropotamus metaflysch west of Koskinon, along the main road from Aliveri to Karystos, the older S_2 is crenulated. The S_3 crenulation cleavage became more intense as it rotated S_2 to produce S–C fabrics, in which S_2 forms the S-planes and S_3 the C-planes (Fig. 10a). This type of D_2–D_3 S–C

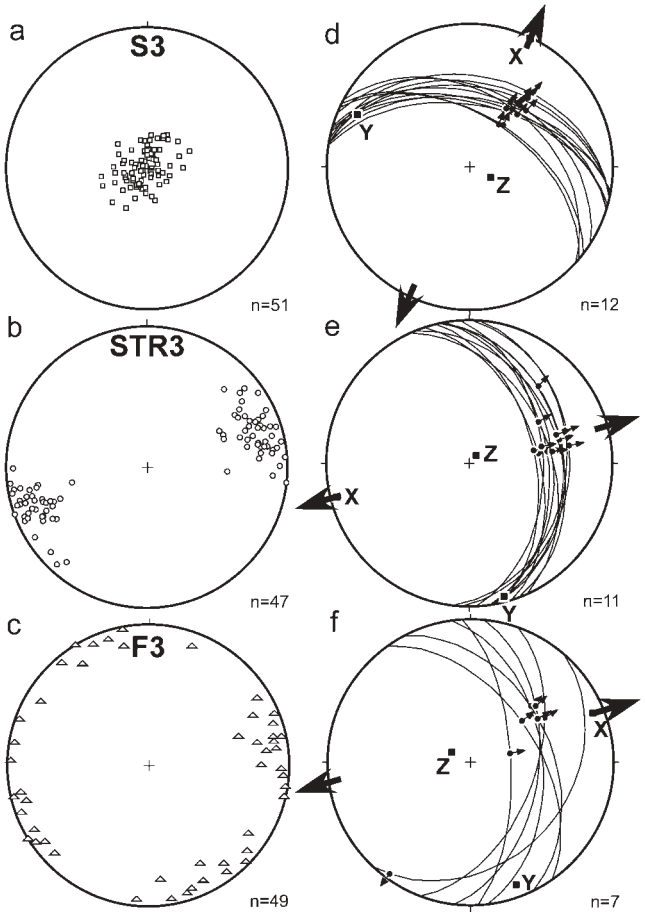

Fig. 8. Stereographic, lower-hemisphere projections of (**a**) S_3, (**b**) STR_3, (**c**) F_3. (**d**–**f**) D_3 fault-slip data from west of Koskinon (**d**), NW of Tsaki (**e**) and SW of Tsaki (**f**); Localities where fault-slip data were obtained are shown in Figure 9.

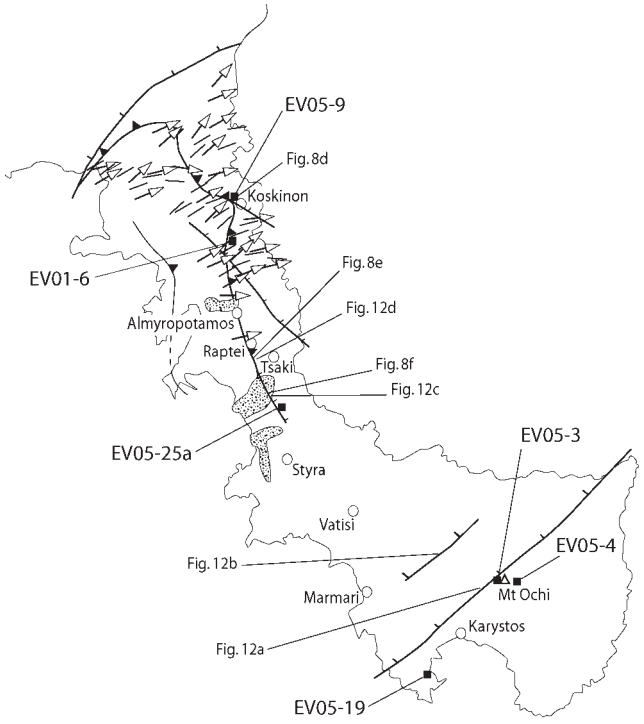

Fig. 9. Map showing STR_3; arrowheads indicate sense of shear associated with STR_3. It should be noted that subhorizontal D_3 structures are localized at the Evia thrust and grade into steep normal faults associated with Neogene basins.

structures formed only locally, because the pre-existing S_2 was in the shortening field of later D_3 shearing. At the northern end of this flysch outcrop, blueschist of the Styra Nappe is in normal-fault contact with the Almyropotamos metaflysch (Fig. 8d). Top-to-the-NE or -ENE D_3 normal faults are common in the Almyropotamos metaflysch (Fig. 10b) and reflect a later stage of D_3 extension.

East of Raptei, D_3 shear bands (Fig. 10d) are pervasive and, in places, cut earlier D_2 isoclinal faults. In some outcrops above the Evia thrust alternating top-to-the-WSW and top-to-the-ENE kinematic indicators occur. In several cases no consistent over-printing relationships could be mapped; however, in a few cases very localized top-to-the-ENE shear bands cut more penetrative, mylonitic top-to-the-WSW shear bands and developed along the same mylonitic foliation (Fig. 10e). The top-to-the-ENE shear bands are characterized by pronounced chlorite growth and quartz recrystallization. The ductile deformation structures show a progressive evolution into semi-ductile and brittle structures, and albite porphyroclasts and quartz show brittle micro-normal faults at moderate to high angles to the tectonic foliation; Riedel structures are also common. In the breccia-filled Riedel structures, very fine-grained chlorite is ubiquitous and albite is severely altered to sericite. The top-to-the-ENE shear bands and breccia-decorated Riedel structures grade into D_3 normal faults (Fig. 10f).

As shown above, the overprinting of D_2 structures by D_3 shows two distinctly different types. By far the most common type is that recorded east of Raptei in which the new D_3 flattening plane is in the extension field of the earlier S_2 planes, leading to transposition and strengthening of S_2 during D_3 and the development of STR_3 on former S_2 planes (Fig. 11). Locally, in the hinge zone of isoclinal D_2 folds, the earlier D_2 planes are in the shortening field of D_3, which produced the D_2–D_3 structures described above from the Almyropotamos metaflysch (Figs 10a and 11).

In serpentinite quarries immediately above the Evia thrust west of Tsaki, top-to-the-WSW S–C structures are cut by top-to-the-ENE shear bands and top-to-the-ENE high-angle normal faults (Fig. 10c). The normal faults can be traced into the Neogene sedimentary basin SW of Tsaki (Fig. 2) and are characterized by ENE–WSW-oriented extension (Fig. 8e and f). Across some of the small-scale normal faults, sandstone layers show thickness changes, with thicker beds on the hanging-wall side of the normal fault.

Xypolias *et al.* (2003) reported asymmetric quartz *c*-axis fabrics from the contact zone between the Styra and Almyropotamos nappes yielding a consistent top-to-the-ENE sense of shear. We interpret these fabrics to reflect localization of lower greenschist-facies mylonitic top-to-the-ENE shearing along the former Evia thrust.

Neotectonic faulting

Young faulting is expressed by linear fault scarps. The fault zones are characterized by fault gouge, which is usually a few metres thick. The fault planes are best developed in marble and

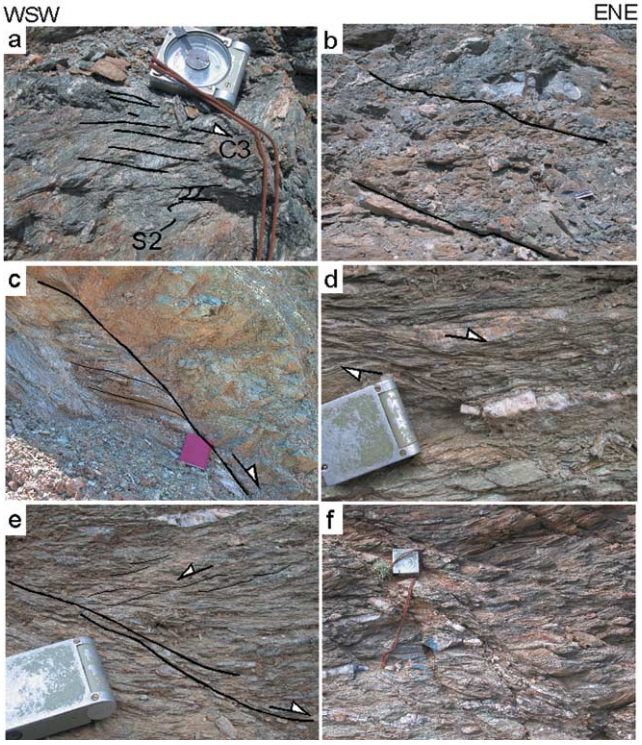

Fig. 10. (**a**) Crenulation of S_2 and progressive development of D_3 S–C-type fabrics. It should be noted that S_2 makes up S-planes and S_3 C-planes; Almyropotamos metaflysch west of Koskinon (38°23′03″N, 24°09′00″E). (**b**) Brittle top-to-the-NE-displacing normal faults in metaflysch of the Almyropotamos Nappe west of Koskinon (38°22′58″N, 24°09′03″E) overprinting earlier structures. (**c**) Top-to-the-ENE normal fault in serpentinite of the Styra Nappe SW of Tsaki. (**d**) Top-to-the-ENE shear bands in metapelite east of Raptei (38°14′37″N, 24°13′55″E); top-to-the-ENE shear bands developed during lower greenschist- to sub-greenschist-facies conditions. (**e**) Localized top-to-the-ENE shear bands cutting top-to-the-WSW shear bands. It should be noted that no new S_3 foliation developed; same outcrop as (**d**). (**f**) Top-to-the-ENE shear bands cut by top-to-the-ENE normal faults in metapelite of the Styra Nappe; normal faults show similar kinematics to top-to-the-ENE shear-sense indicators in the same outcrop (38°14′49″N, 24°14′07″E).

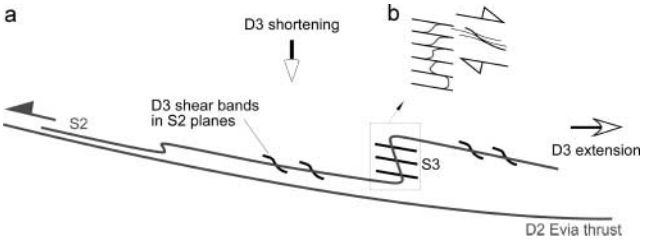

Fig. 11. Sketch illustrating two types of D_2–D_3 overprinting. (**a**) The most common type is that new D_3 flattening plane is in the extension field of older S_2 planes, leading to transposition and strengthening of S_2 during D_3. (**b**) In hinge zones of isoclinal D_2 folds, earlier D_2 planes are in the shortening field of D_3, producing D_2–D_3 structures as shown in Figure 10a.

contain millimetre-scale frictional-wear striae and decimetre-scale corrugations. In the footwalls of the main fault planes are arrays of minor striated faults coated with centimetre-thick fault gouges.

A prominent, young NW-dipping fault runs along the north-western side of Mt. Ochi (Figs 2 and 3). The Mt. Ochi block in the footwall of the fault has an altitude of up to *c*. 1400 m and is the most prominent geomorphological feature in southern Evia. This prominent uplift is due to young faulting, which also caused offset of the Quaternary gravel in the Karystos Basin. The fault zone in the high topography near Mt. Ochi is diffuse and obscured by landsliding.

Fault-slip data show dextral normal faulting as a result of approximately north–south extension (Fig. 12a). A minor fault near Paradisi strikes subparallel to the Mt. Ochi fault and yielded similar kinematic data (Fig. 12b).

Another set of young faults strikes NW–SE, almost perpendicular to the Mt. Ochi fault. We mapped two faults of this set near Tsaki (Fig. 2). Both faults formed during the D_3 extensional event and were reactivated during neotectonic faulting, as evidenced by cross-cutting striations on fault planes and over-printing relationship of minor faults. Both datasets show normal faulting on NE-dipping planes with a modest sinistral oblique-slip component (Fig. 12c and d).

Geochronology

The structural work showed that the sense of shear during D_2 shows a systematic reversal from top-to-the-WSW at the Evia thrust to top-to-the-ENE at the Mt. Ochi shear zone. To determine whether the absolute timing of these shears is the same we carried out Rb–Sr dating of mylonites at both contacts. Furthermore, we report fission-track data that clarify the subse-

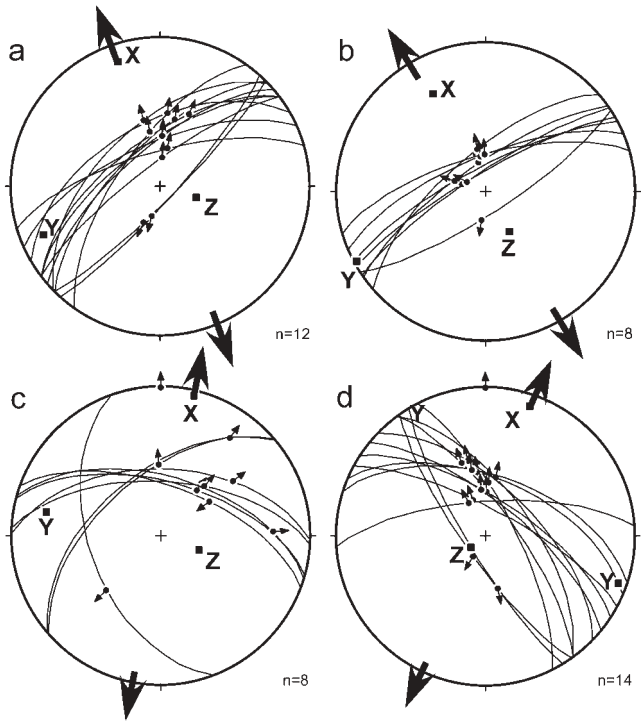

Fig. 12. Fault-slip analysis of young faults. (**a**) Data from the Mt. Ochi fault characterized by NW-dipping dextral oblique normal faults. (**b**) Small-scale fault near Paradisi yielding similar data to the Mt. Ochi fault. (**c**) Young reactivation of a normal fault in the Neogene basin SW of Tsaki yielding NNE–SSW-oriented extension. (**d**) Young reactivation of a normal fault north of Tsaki indicating NNE–SSW-oriented extension. Localities where fault-slip data were obtained are shown in Figure 9.

quent cooling history. The localities of the geochronological samples are shown in Figure 9.

Rb–Sr dating

Method. For Rb–Sr analysis the internal mineral isochron approach was used (Glodny *et al*. 2002, 2005). Small samples (*c*. 20–100 g) have been chosen, the assemblages of which can be clearly tied to certain tectonic or metamorphic events. The samples for the present study are three strongly deformed blueschist-facies mylonites and one greenschist-facies albite–epidote–white mica schist, all showing a minimum of post-metamorphic alteration. The Rb–Sr system of white mica is thermally stable to temperatures >500–550 °C but may be fully reset by dynamic recrystallization (Inger & Cliff 1994; Freeman *et al*. 1997; Villa 1998). Isotopic re-equilibration between white mica and coexisting phases during mylonitization can occur at temperatures as low as 350 °C (Müller *et al*. 1999). Careful study of the correlation between microtextures and isotopic signatures, both by conventional mineral separation techniques (Müller *et al*. 1999) and by Rb–Sr microsampling (Müller *et al*. 2000; Cliff & Meffan-Main 2003) has shown that complete synkinematic recrystallization in mylonites is usually accompanied by isotopic re-equilibration. Therefore, Rb–Sr isotopic data from penetratively deformed rocks can be used to date the waning stages of mylonitic deformation, provided that deformation occurred below the temperature range at which diffusional resetting is activated. In our samples, late increments of deformation and related white mica recrystallization occurred at temperatures well below 500–550 °C, which ensures that Rb–Sr isotopic signatures record deformation or greenschist-facies recrystallization. To detect possible Sr-isotopic inhomogeneities resulting from long-term incomplete dynamic recrystallization, from diffusional Sr redistribution and/or from alteration processes, white mica was analysed in several, physically different (in terms of magnetic properties and/or grain size) fractions whenever possible. This approach ensures control on possible presence of unequilibrated, pre-deformational white mica relics (see Müller *et al*. 1999).

White mica fractions were ground in ethanol in an agate mortar and then sieved in ethanol to obtain pure, inclusion-free separates. All mineral concentrates were checked and finally purified by hand-picking under a binocular microscope. Rb and Sr concentrations were determined by isotope dilution using mixed ^{87}Rb–^{84}Sr spikes. Determinations of Rb and Sr isotope ratios were carried out by thermal ionization mass spectrometry (TIMS) on a VG Sector 54 multicollector instrument (GeoForschungsZentrum Potsdam). Sr was analysed in dynamic mode. The value obtained for $^{87}Sr/^{86}Sr$ of NBS standard SRM 987 was 0.710268 ± 0.000015 ($n = 19$). The observed ratios of Rb analyses were corrected for 0.25% per a.m.u. mass fractionation. Total procedural blanks were consistently below 0.15 ng for both Rb and Sr. Because of generally low and highly variable blank values, no blank correction was applied. Isochron parameters were calculated using the Isoplot/Ex program of Ludwig (1999). Standard errors, as derived from replicate analyses of spiked white mica samples, of ±0.005% for ^{87}Sr–^{86}Sr ratios and of ±1.5% for Rb–Sr ratios were applied in isochron age calculations. Individual analytical errors were generally smaller than these values.

Description of samples. Samples EV05-3 and EV05-4 are from the Mt. Ochi normal shear zone (lowermost Ochi Nappe) and sample EV05-9 is from the Evia thrust (lowermost Styra Nappe) (Figs 2 and 3). EV05-4 is a fine-grained glaucophane mylonite, with phengite, albite, quartz, epidote and accessory apatite; EV05-3 and EV05-9 are fine-grained glaucophane and phengite-bearing quartz mylonites with additional chlorite, albite and apatite. The very strong mylonitization caused complete recrystallization of phengite, glaucophane, apatite and other minerals (Fig. 13) and only a single generation of a mineral is present in each dated sample. The very fine-grained nature of the mylonite indicates that there are no compositional heterogeneities across the crystals.

Sample EV05-25A is a greenschist-facies albite–epidote–white mica schist from the lower Styra Nappe that also contains chlorite, quartz, titanite and opaque minerals. This sample is from an outcrop of D_2 top-to-the-WSW shear (see above). Texturally, sample EV05-25A is heterogeneous and contains (1) epidote-rich and (2) plagioclase- and opaque-rich domains. Domain (1) has a weak but discernible greenschist-facies

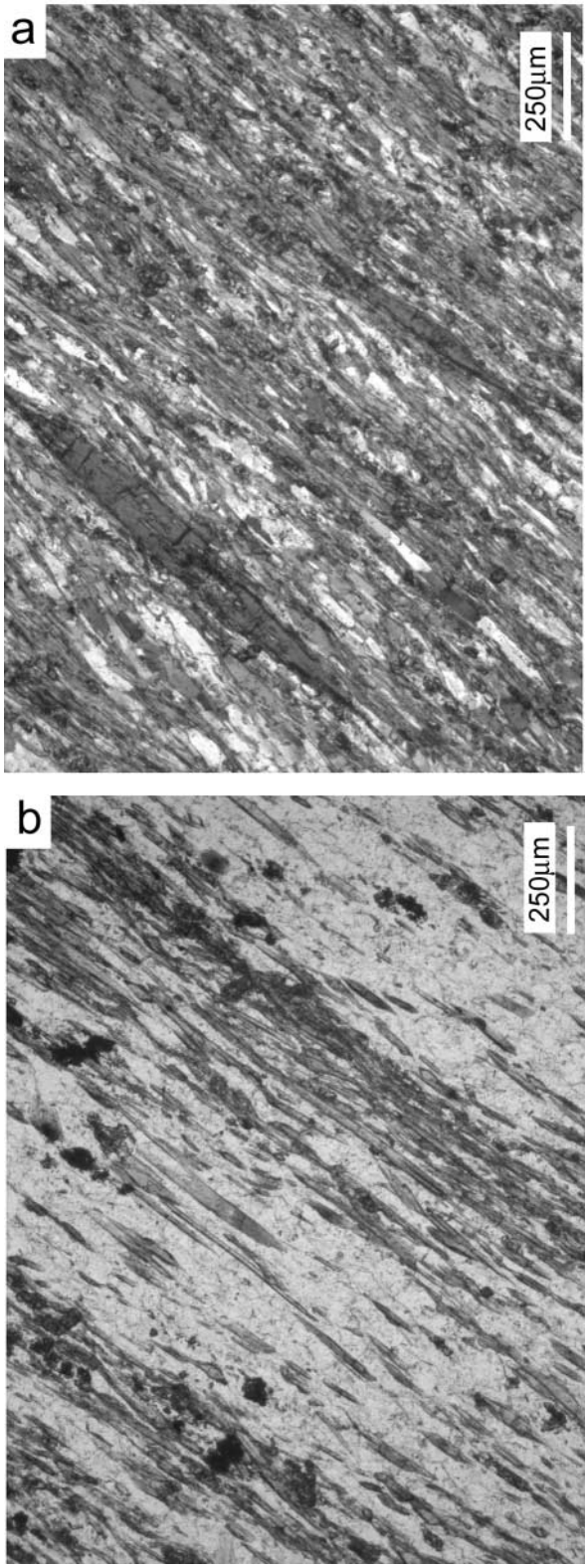

Fig. 13. Photomicrographs of thin sections of mylonite samples EV05-3 (**a**, crossed polars) and EV05-4 (**b**, plane-polarized light) (for sample locations refer to Fig. 9); penetrative mylonitic deformation occurred under blueschist-facies conditions in the stability field of glaucophane (long-prismatic minerals); phengite is present as fine synkinematic fibres; the absence of pre-deformational textural relics should be noted.

foliation that is defined by weakly aligned epidote porphyroblasts and white mica. Commonly, domain (2) is unfoliated; in places nematoblastic opaque phases outline a faint shape-preferred orientation. White mica occurs in both domains as randomly oriented, fine-grained minerals, some of which grew obliquely to the weak foliation and, in small areas, as foliation-forming minerals. From textural observations it appears unlikely that the micas grew at different times. Rather, heterogeneous deformation and strain partitioning led to local mica (re?)crystallization and alignment in the strained domains and random growth in strain shadows.

Data. Rb–Sr geochronology of the high-pressure mylonites yielded strikingly consistent age information from the Mt. Ochi normal shear zone and the Evia thrust. Deformation ages have been calculated using Rb–Sr data for white mica and cogenetic phases such as epidote, glaucophane, feldspar and apatite.

From the Mt. Ochi normal shear zone we obtained a well-defined five-point isochron age of 33.0 ± 1.0 Ma (all reported errors are quoted at the 2σ level) for sample EV05-3 and a three-point isochron age of 27.2 ± 0.9 Ma for EV05-4 (Table 1, Fig. 14a and b). Both ages are interpreted to reflect final stages of mylonitization-related isotopic re-equilibration under blueschist-facies conditions. It appears that deformation at blueschist-facies conditions within the Mt. Ochi normal shear zone occurred during a prolonged period, at least in the period bracketed by our two deformation ages.

A three-point isochron age of sample EV05-9 from the Evia thrust zone yielded an age of 29.5 ± 0.3 Ma (Table 1, Fig. 14c), which is again interpreted to reflect final stages of mylonitization-related isotopic re-equilibration under blueschist-facies conditions. The age of 29.5 ± 0.3 Ma is similar to the $^{40}Ar-^{39}Ar$ white mica mylonitization ages of *c*. 35–30 Ma from the Evia thrust reported by Maluski *et al*. (1981) and Ring & Layer (2003).

Sample EV05-25a yielded a four-point isochron age of 20.9 ± 0.3 Ma (Table 1, Fig. 14d). We interpret this age to date fluid-assisted late-D_2 recrystallization under greenschist-facies conditions. Therefore, the age of 20.9 ± 0.3 Ma is very close to the end of D_2 ductile shearing.

Fission-track dating

Method. Apatite and zircon crystals were separated, mounted, polished and etched according to the techniques outlined by Hurford & Green (1982). The samples were analysed applying the external detector method and irradiated at the Oregon State University Triga Reactor, Corvallis, USA. The neutron fluence was monitored using Corning uranium-dosed glasses CN5 and CN2. Spontaneous and induced fission-track densities were counted using an Olympus BX51 microscope at 1250× magnification. A CN2 zeta-calibration factor of 130.7 ± 2.8 Ma (zircon) and 356.1 ± 15.3 (apatite) was obtained by repeated calibration against a number of internationally agreed age standards according to the recommendations of Hurford (1990). The closure temperature for fission tracks in zircon at moderate to fast cooling rates is 110 ± 10 °C for apatite (Green *et al*. 1986) and 280 ± 30 °C for zircon (Stöckhert *et al*. 1999).

Data. We obtained a zircon fission-track age of 17.8 ± 0.9 Ma for sample EV01-6 from the lowermost Styra Nappe (Table 2). Apatite from leucogranite sample EV05-19 from the upper Styra Nappe was analysed twice. We consider the age of 8.4 ± 3.3 Ma of the replicate sample as the best date for cooling of the Styra Nappe below 110 ± 10°C.

Together with the age of *c*. 21 Ma for greenschist-facies deformation (below *c*. 350 °C) the zircon fission-track age provides a moderate cooling rate of *c*. 10–15 °C Ma^{-1} for the Styra Nappe in the Early Miocene. The cooling rate as derived from the zircon and apatite fission-track ages for the period from *c*. 18 Ma to *c*. 8 Ma is not significantly different (*c*. 12–25 °C Ma^{-1}).

Tectonic interpretation

Oligocene extrusion wedge

The kinematic indicators associated with D_2 show a systematic reversal from top-to-the-WSW in the basal parts of the Styra Nappe and in the Almyropotamos Nappe to top-to-the-ENE in higher levels of the Styra Nappe and in the Ochi Nappe. Our Rb–Sr mylonitization ages, together with the age data of Maluski

Table 1. *Rb–Sr analytical data*

Sample and analysis number	Material	Rb (ppm)	Sr (ppm)	$^{87}Rb/^{86}Sr$	$^{87}Sr/^{86}Sr$	$^{87}Sr/^{86}Sr$ $2\sigma_m$ (%)
Blueschist-facies rocks						
EV05-9 (quartz-rich mylonite; 29.5 ± 0.3 Ma; MSWD <1, $Sr_i = 0.71060 \pm 0.00012$*)*						
PS1342	Glaucophane	10.7	2.05	15.1	0.716930	0.0046
PS1336	Wm 125–90 μm	268	1.82	433	0.891893	0.0018
PS1334	Wm 250–160 μm	270	1.83	434	0.892665	0.0028
EV05-4 (blueschist; 27.2 ± 0.9 Ma, MSWD <1, $Sr_i = 0.704921 \pm 0.000025$*)*						
PS1340	Glaucophane	1.72	33.4	0.149	0.704978	0.0016
PS1339	Wm conc.	54.4	42	3.74	0.706363	0.0018
PS1337	Epidote	1.49	1070	0.00402	0.704922	0.0014
EV05-3 (quartz-rich mylonite; 33.0 ± 1.0 Ma, MSWD = 1.6, $Sr_i = 0.706484 \pm 0.000031$*)*						
PS1302	Wm 180–125 μm	122	117	3.02	0.707865	0.0035
PS1305	Wm 355–250 μm	109	126	2.50	0.707674	0.0012
PS1333	Wm 250–180 μm	117	128	2.66	0.707745	0.0014
PS1338	Apatite	2.60	752	0.100	0.706480	0.0018
PS1341	Glaucophane	5.16	11.3	1.32	0.707110	0.0016
Greenschist-facies rocks						
EV05-25a (epidote greenschist; 20.9 ± 0.3 Ma, MSWD = 1.6, $Sr_i = 0.706112 \pm 0.000025$*)*						
PS1390	Epidote	3.50	1034	0.00979	0.706095	0.0014
PS1396	Wm 63–90 μm	147	26.4	17.2	0.711248	0.0014
PS1398	Feldspar (+ quartz)	2.33	13.7	0.493	0.706281	0.0014
PS1401	Wm 160–90 μm	137	32.6	12.2	0.709714	0.0014

Uncertainty of ±1.5% (2σ) has to be assigned to Rb–Sr ratios; typical sample weights are 0.5–5 mg for apatite and epidote, and 5–15 mg for feldspar, amphibole and white mica. Wm, white mica.

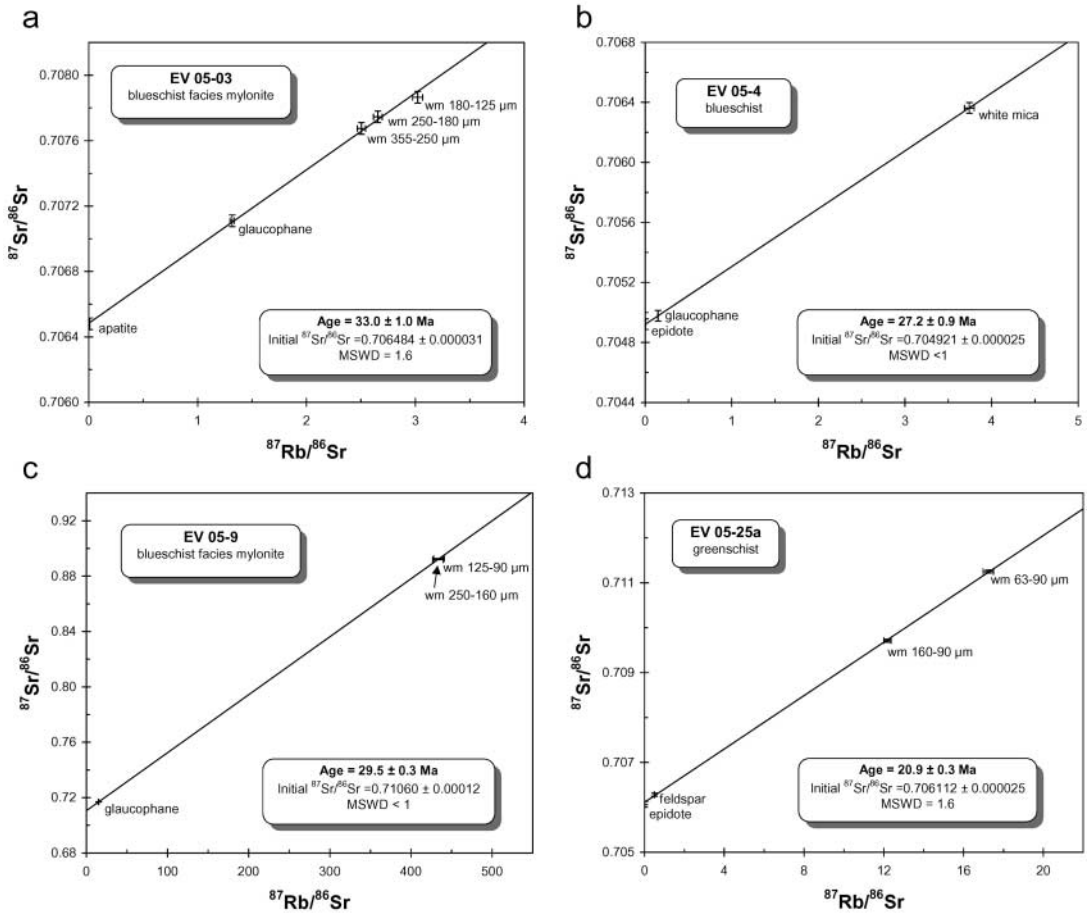

Fig. 14. Rb–Sr isochron diagrams; all errors are 2σ. (**a**) Five-point isochron age of 33.0 ± 1.0 Ma for sample EV05-3 (38°03′34″N, 24°28′00″E). (**b**) Data for sample EV05-4 form a three-point isochron of 27.2 ± 0.9 Ma (38°03′47″N, 24°28′03″E). (**c**) Three-point isochron age of 29.5 ± 0.3 Ma for sample EV05-9 from the Evia thrust (38°22′58″N, 24°09′03″E). (**d**) Sample EV05-25a (38°12′54″N, 24°14′43″E) yielded a four-point isochron age of 20.9 ± 0.3 Ma for fluid-assisted late-D_2 recrystallization under greenschist-facies conditions. (For sample locations refer to Fig. 9.)

Table 2. *Fission-track data*

Sample number	Elevation (m)	Rock type (Unit/nappe)	Mineral	Number of crystals	Track density ($\times 10^6$ tracks cm^{-2})			Age dispersion ($P\chi^2$)	Central age (Ma) (±1σ)
					ρ_s (N_s)	ρ_i (N_i)	ρ_d (N_d)		
EV01-6	112	Schist, Styra Nappe	Zircon	20	2.606 (925)	4.009 (1423)	41.92 (5790)	<0.01% (98%)	17.8 ± 0.9
EV05-19	11	Leucogranite, Styra Nappe	Apatite	8	0.03601 (4)	0.5941 (178)	1.238 (3863)	0.02% (71%)	13.4 ± 6.9
EV05-19 RP	11	Leucogranite, Styra Nappe (replicate analysis)	Apatite	16	0.03334 (7)	0.8822 (185)	1.227 (3830)	37.2% (27.3%)	8.4 ± 3.3

Analyses were by external detector method using 0.5 for the $4\pi/2\pi$ geometry correction factor. Ages were calculated using dosimeter glass: CN2 with $\zeta_{CN2} = 130.7 \pm 2.8$ (zircon); CN5 with $\zeta_{CN5} = 356.1 \pm 15.3$ (apatite). $P\chi^2$ is the probability of obtaining a χ^2 value for ν degrees of freedom, where ν = number of crystals − 1.

et al. (1981) and Ring & Layer (2003), indicate that the D_2 event commenced under blueschist-facies conditions between *c*. 33 and 30 Ma and ultimately caused high-pressure metamorphism in the underlying Almyropotamos nappe at *c*. 23 Ma. According to van Hinsbergen *et al*. (2005*b*), the shear direction has to be back-rotated anticlockwise by *c*. 50° into its original position. The mean of STR_2 trends N66°E and if backrotated would result in an Oligocene and Early Miocene NNE–SSW trend; that is, the structures in the lower half of the nappe pile would record top-to-the-SSW movement and those in the higher levels top-to-the-NNE movement.

Deformation–metamorphism relationships indicate that the D_2 structures in the basal Styra Nappe started to develop under blueschist-facies conditions and brought the Styra Nappe on top of the Almyropotamos Nappe along the Evia thrust. We regard the relict D_1 structures as an early increment of D_2. D_2 also caused internal imbrication of the Almyropotamos Nappe along the Almyropotamos thrust. The fact that the Evia thrust put the higher-pressure Styra Nappe above the lower-pressure Almyropotamos Nappe and that this deformation resulted in deep burial of the Almyropotamos Nappe leads us to conclude that D_2 top-to-the-SSW movement resulted from horizontal shortening. Furthermore, D_2 is intimately related to the deposition and deformation of the Almyropotamos flysch. The flysch needs to be associated

with crustal thickening, the development of topography and associated erosion, and the formation of olistoliths. Thrusting-related flysch deposition in the External Hellenides (Richter *et al*. 1978; van Hinsbergen *et al*. 2005*a*) coincides well with the envisaged timing of D_2 thrusting and deposition of the Almyropotamos metaflysch.

The top-to-the-NNE kinematic indicators in the higher levels of the nappe pile occur in the same subhorizontal foliation as the top-to-the-SSW kinematic indicators in the lower levels. Deformation–metamorphism relationships also suggest that the top-to-the-NNE structures started to form under high-pressure conditions. In the central parts of the Styra Nappe, between Styra and Vatisi, mutual overprinting relations between top-to-the-SSW and top-to-the-NNE kinematic indicators occur. These features strongly suggest that the two sets of shear-sense indicators formed contemporaneously. Moreover, if the top-to-the-SSW kinematic indicators resulted from crustal shortening, then top-to-the-NNE movement must be related to normal-sense shearing. This view is further corroborated by the progressive evolution from subhorizontal ductile top-to-the-NNE structures to semi-brittle and steep brittle structures in the Mt. Ochi normal shear zone. The fault-slip data indicate that the kinematics of deformation during falling temperatures and progressive steepening of the D_2 top-to-the-NNE structures remained unchanged. This progressive steepening and the consistent dip of the steep brittle D_2 faults strongly suggest that these structures were not rotated about horizontal axes to any significant degree and therefore resulted from normal faulting.

Above, we showed that the top-to-the-SSW thrust-related high-pressure mylonites in the lower Styra Nappe formed at *c*. 33–30 Ma. The top-to-the-NNE normal structures that formed during the same high-pressure metamorphism should be similar in age, and our Rb–Sr ages for the final stages of high-pressure mylonitzation indeed yielded ages of 33–27 Ma. Our Rb–Sr data also indicate that greenschist-facies mineral growth associated with the latest increments of shearing at *c*. 21 Ma dates the waning stages of D_2 thrusting. The latter age agrees with the age for high-pressure metamorphism in the underlying Almyropotamos Nappe of *c*. 23 Ma and is corroborated by largely similar P–T conditions for the greenschist-facies overprint in the Ochi Nappe and the high-pressure metamorphism in the Almyropotamos Nappe (Katzir *et al*. 2000; Shaked *et al*. 2000). The age of *c*. 21 Ma fits also well with the end of flysch deposition in the External Hellenides and folding and uplift of the external Hellenic equivalent of the Almyropotamos Nappe (van Hinsbergen *et al*. 2005*a*).

We envisage that high-pressure metamorphism in the Almyropotamos Nappe released fluids that moved upwards, causing retrograde, fluid-assisted metamorphic reactions in the overlying, emplacing Styra and Ochi nappes. The age of *c*. 21 Ma for the end of D_2 thrusting and the greenschist-facies P–T estimates of Katzir *et al*. (2000) indicate that >2–4 kbar of exhumation was accomplished in *c*. 6–12 Ma. These crude estimates translate into exhumation rates of *c*. 0.5–2 km Ma^{-1} for the basal Styra Nappe in the ductile crust.

The Mt. Ochi normal shear zone shows a structural development from ductile conditions in the Mt. Ochi area to distinctly brittle–ductile and brittle conditions around Kavo Doro (Fig. 5). Large-scale normal faults in the Aegean that show such a progressive evolution from ductile to brittle conditions usually have the Upper Unit in their hanging wall. The Upper Unit is not exposed on Evia, but the structural relationships predict that it should be sought to the east of Evia and, thus, on Andros (Fig. 1). The Makrotantalon Nappe is exposed on westernmost Andros, opposite Evia, and is considered to correspond to the Upper Unit (Papanikolaou 1978). Dürr (1986) regarded the basal contact of the Makrotantalon Nappe as a low-angle normal fault, and our field observations are in line with top-to-the-ENE normal faulting (U. Ring, unpubl. data). This contact is decorated and directly underlain by a series of serpentinite lenses, which may correlate to the serpentinites of the Ochi Nappe. This interpretation implies that the entire Ochi Nappe is a heterogeneous normal shear zone.

Our tectonic interpretation of the D_2 structures argues for the development of an extrusion wedge made up by the Styra Nappe and bounded by the Evia thrust at its base and the Mt. Ochi normal shear zone at its top. The normal-sense shearing is a geometric effect only and probably not due to net extension of the region during inception of D_2 in the mid-Oligocene. In the easternmost Aegean, Ring *et al*. (2007) described an extrusion wedge, consisting of a nappe that is correlative to the Styra Nappe, and dated the bounding faults at 42–32 Ma. In contrast, deformation on the bounding faults of the extrusion wedge on Evia started *c*. 10 Ma later but was also active for about 10 Ma. The age difference of *c*. 10 Ma between the western and eastern Aegean is probably due to lateral changes in the orogenic architecture: underthrusting of the External Hellenides in the western Aegean did not commence before the Oligocene, whereas underthrusting of the Menderes Nappes in the easternmost Aegean and western Turkey had already commenced in the Eocene.

There is another major difference between the extrusion wedge described here from Evia and the one reported from the easternmost Aegean and western Turkey by Ring *et al*. (2006). On Evia, the normal fault at the top of the extrusion wedge shows a progressive evolution from high-pressure metamorphism and ductile deformation to brittle conditions. Furthermore, the Upper Unit occurs in the hanging wall of the normal fault; that is, it operated from *c*. 40 km depth all the way up into the brittle crust. In the easternmost Aegean, however, the normal-sense shear zone at the top of the extrusion wedge apparently stopped operating at greenschist-facies conditions, and there is no high-level tectonic unit in the hanging wall of the normal fault (Ring *et al*. 2007). The final exhumation of the Cycladic Blueschist Unit in the easternmost Aegean and western Turkey from mid-crustal levels was accomplished by Miocene and Pliocene extensional faults (Gessner *et al*. 2001c; Ring *et al*. 2003*b*; Kumerics *et al*. 2005).

The shortening structures that emplaced the extrusion wedges on Evia and in the easternmost Aegean (Ring *et al*. 2007) are from the western and eastern margin of the Aegean Sea and apparently are preferentially preserved there. It seems that the very strong Miocene extensional deformation in the central Aegean, which on Naxos and Paros was associated with high-grade metamorphism that locally reached anatexis, erased most or all of the earlier structures.

Miocene thrusting

Kokkalas (2001) and Xypolias *et al*. (2003) argued that the Kimi thrust is associated with the accumulation of the lower sequence of the Kimi Basin and thus Early Miocene in age. This shortening event occurred at high structural levels and probably postdates the Oligocene extrusion wedge. We suggest that the Kimi thrust formed during a shortening event that was coeval with slow cooling after greenschist-facies deformation in the Styra Nappe. We realize that this conclusion is speculative. It is also conceivable that deformation at the Evia, Almyropotamos and Kimi thrusts resulted from prolonged crustal shortening that

commenced in the Early Oligocene during high-pressure metamorphism in the Styra Nappe and continued until the Middle Miocene.

Late extension

D_3 top-to-the-ENE structures mainly formed in the vicinity of the Evia thrust (Fig. 9). The D_3 structures started to form under greenschist-facies conditions and evolved into steep brittle normal faults associated with the development of the Middle to Late Miocene basins. There is evidence for synsedimentary normal faults in the sediments. Similar arguments as used above for the D_2 top-to-the-NNE structures strongly suggest that the D_3 top-to-the-ENE structures resulted from horizontal extension. This extension mainly reactivated the Evia thrust as a low-angle normal fault. The D_2–D_3 overprinting fabrics indicate that the D_2 structures were commonly in the extension field of subsequent D_3, leading to the development of prominent D_3 extensional fabrics. The deformation–metamorphism relationships indicate that this extensional event exhumed the Almyropotamos Nappe from *c*. 35 km depth. Kokkalas (2001) and Xypolias *et al*. (2003) argued that extensional structures resulting from ENE–WSW-directed extension in the Kimi Basin started to form after the Middle Miocene and controlled the deposition of the upper sequence of the Kimi Basin. The timing constraints suggest that D_3 extension started after *c*. 15 Ma and thus at the time when the *c*. 40° clockwise rotation commenced (*c*. 14 Ma) and the Oxylithos volcanic rocks crystallized (15–13 Ma). We argue that the strong clockwise rotation was coeval with D_3 extension and the development of the magmatic arc (Oxylithos volcanic rocks) of the southward retreating Hellenic subduction zone in Evia. Elsewhere in the Aegean, the magmatic-arc stage is associated with strong horizontal extension and detachment faulting (Lister *et al*. 1984; Faure *et al*. 1991; Ring *et al*. 2003*a*; Kumerics *et al*. 2005; Brichau *et al*. 2006). Ring *et al*. (1999*c*) argued that Miocene extensional deformation on Samos in the eastern Aegean was associated with pronounced anticlockwise rotation in a sinistral wrench corridor. Likewise, the Late Miocene extensional structures on Evia at the western end of the Aegean Sea may have formed in a dextral wrench corridor. This all fits into a picture of pronounced outward migration of the central part of the Hellenic subduction zone, associated with clockwise rotation in the western Aegean and anticlockwise rotation in the eastern Aegean (Kissel *et al*. 1986). Consequently, southward trench retreat of the Hellenic subduction zone since the Miocene must have been restricted to the central section of the Hellenide–Anatolian orogen (Ring & Layer 2003) (Fig. 15).

Neotectonic faulting

Young faulting is expressed by two sets of conjugated faults, which strike almost perpendicular to each other. Both fault sets resulted from *c*. NNE–SSW extension and probably belong to a system of seismically active neotectonic faults related to the southwestward propagation of the dextral North Anatolian fault and the opening of the South Evia Rift and the Corinth Rift (Ganas *et al*. 2005). The kinematics of extension in Evia, recorded by the striations and corrugations on outcropping

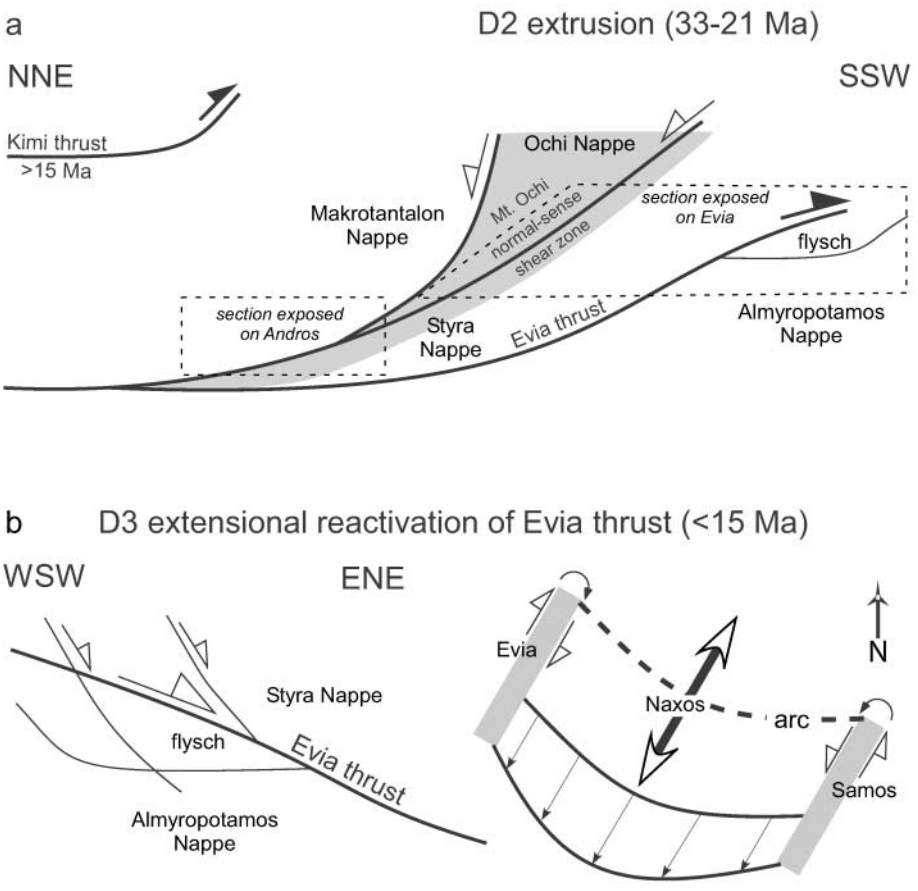

Fig. 15. Summary of tectonic interpretation. (**a**) Oligocene extrusion wedge stage. Thrusting of the Cycladic Blueschist Unit onto the Basal Unit commenced at *c*. 35–30 Ma and caused high-pressure metamorphism in the Almyropotamos Nappe at *c*. 23 Ma. This shortening event may have also caused internal imbrication within the Cycladic Blueschist Unit but the Ochi Nappe subsequently became a normal shear zone that exhumed the Styra Nappe from *c*. 33 Ma onwards. Normal shearing became inactive at *c*. 21 Ma, as is corroborated by slow cooling in the Styra Nappe from 21 Ma onwards. The brittle normal detachment of the extrusion wedge is supposed to be the base of the Makrotantalon Nappe on Andros. Grey boxes approximately indicate the exposed crustal sections on Evia and Andros. The Kimi thrust formed later and may or may not be result of the same shortening event that caused high-pressure metamorphism in the Almyropotamos Nappe. (**b**) D_3 top-to-the-ENE extensional reactivation of the Evia thrust in cross-section. The map view interprets dextral and sinistral wrench corridors at both ends of Aegean Sea basin as an accommodation feature of spatially limited southward retreat of the subducting slab. The magmatic arc arrived in the northern Cyclades between Evia and Samos after *c*. 15 Ma.

faults, is identical to that described by global positioning system and focal-mechanism data (Taymaz *et al*. 1991; Davies *et al*. 1997). Figure 1 (insert 2) shows a simplified pattern of conjugated, seismically active faults in the central Aegean. Kiratzi & Louvari (2003) argued that the NE–SW-trending faults are related to the westward propagating North Anatolian fault. In northern Turkey, this fault strikes east–west and has almost pure dextral strike-slip kinematics. When entering the Aegean Sea, the North Anatolian fault curves into a NE–SW orientation and the faults have an additional normal-slip component. The second set of neotectonic faults strikes NW–SE and has almost pure dip-slip kinematics associated with prominent rifts zones. The very thin crust south of Evia is spatially related to these conjugated fault sets.

Conclusions

The aim of this study was to test whether there is evidence for an extrusion wedge aiding the early exhumation of the Cycladic Blueschist Unit on Evia through an investigation of the interplay between crustal shortening, high-pressure metamorphism, normal faulting and exhumation. The most important finding of our work is the evidence for an Oligocene extrusion wedge that accomplished the early exhumation of the Styra Nappe from depths where it underwent blueschist-facies metamorphism. We provide strong evidence that the Mt. Ochi normal shear zone started to move during peak high-pressure metamorphism at 33–27 Ma. This finding demonstrates the importance of extrusion wedges for the initial exhumation of the Cycladic Blueschist Unit. If, by analogy with the Cycladic Blueschist Unit exposed adjacent to Evia, an age of 55–45 Ma is assumed for high-pressure metamorphism on Evia, our data imply that the blueschists must have stayed at depth for >10–20 Ma before their exhumation started.

We also demonstrate that there is a distinct Middle to Late Miocene extensional event on Evia. The D_3 event caused only moderate exhumation of the Cycladic Blueschist Unit (Styra and Ochi nappes). This is consistent with other results that show that the Middle to Late Miocene extension phase in the Aegean was primarily achieved along low-angle extensional faults that caused considerable extension, and the opening of the Aegean Sea, but did not contribute significantly to the exhumation of the Cycladic Blueschist Unit. However, Miocene normal faulting was important for the exhumation of high-pressure rocks of the External Hellenides (including the Basal Unit and the Cretan high-pressure rocks).

Our data from the neotectonic faults on southern Evia supply additional evidence for the presence of conjugated, seismically active faults that are related to the westward propagation of the North Anatolian fault into the western Aegean. The neotectonic faults are responsible for localized Quaternary basins and final attenuation of the Aegean crust.

This work was funded by the Deutsche Forschungsgemeinschaft (grants Ri538/16, -/18 and -/23). We thank B. Fassoulas for providing information on Andros, D. van Hinsbergen and an anonymous referee for constructive reviews, and H. de Bruijn for age information on the lacustrine deposits of the Kimi Basin.

References

Avigad, D., Garfunkel, Z., Jolivet, L. & Azanon, J.M. 1997. Back arc extension and denudation of Mediterranean eclogites. *Tectonics*, **16**, 924–941.

Brichau, S., Ring, U., Carter, A., Ketcham, R., Brunel, M. & Stockli, D. 2006. Constraining the long-term evolution of the slip rate for a major extensional fault system in the central Aegean, Greece, using thermochronology. *Earth and Planetary Science Letters*, **241**, 293–306.

Cliff, R.A. & Meffan-Main, S. 2003. Evidence from Rb–Sr microsampling geochronology for the timing of Alpine deformation in the Sonnblick Dome, SE Tauern Window, Austria. *In:* Vance, D., Müller, W. & Villa, I.M. (eds) *Geochronology: Linking the Isotopic Record with Petrology and Textures*. Geological Society, London, Special Publications, **220**, 159–172.

Davies, R.P., England, P.C., Parsons, B.E., Billiris, H., Paradissis, D. & Veis, G. 1997. Geodetic strain in Greece in the interval 1892–1992. *Journal of Geophysical Research*, **102**, 24571–24588.

Dubois, R. & Bignot, G. 1979. Présence d'un 'hardground' nummulitique au de la série Cretacée d'Almyropotamos (Eubée méridionale, Grèce). *Comptes Rendus de l'Académie des Sciences, Série II*, **289**, 993–995.

Dürr, S. 1986. Das Attisch – Kykladische Kristallin. *In:* Jacobshagen, V. (ed.) *Geologie von Griechenland*.. Bornträger, Berlin, 116–148.

Dürr, S., Altherr, R., Keller, J., Okrusch, M. & Seidel, E. 1978. The Median Aegean Crystalline Belt: stratigraphy, structure, metamorphism, magmatism. *In:* Cloos, H., Roeder, D. & Schmidt, K. (eds) *Alps, Apennines, Hellenides*. Schweizerbart, Stuttgart, 455–477.

Evans, B.W. 1990. Phase relations of epidote-blueschists. *Lithos*, **25**, 3–23.

Faure, M., Bonneau, M. & Pons, J. 1991. Ductile deformation and syntectonic granite emplacement during the late Miocene extension of the Aegean (Greece). *Bulletin de la Société Géologique de France*, **162**, 3–11.

Freeman, S.R., Inger, S., Butler, R.W.H. & Cliff, R.A. 1997. Dating deformation using Rb–Sr in white mica: greenschist facies deformation ages from the Entrelor shear zone, Italian Alps. *Tectonics*, **16**, 57–76.

Ganas, A., Drakatos, G., Pavlides, S.B., Stavrakakis, G.N., Ziazia, M., Sokos, E. & Karastathis, V.K. 2005. The 2001 Mw = 6.4 Skyros earthquake, conjugate strike-slip faulting and spatial variation in stress with the central Aegean Sea. *Journal of Geodynamics*, **39**, 61–77.

Gautier, P. & Brun, J.-P. 1994. Ductile crust exhumation and extensional detachments in the central Aegean (Cyclades and Evia islands). *Geodinamica Acta*, **7**, 57–85.

Gessner, K., Ring, U., Passchier, C.W. & Güngör, T. 2001a. How to resist subduction: Eocene post-high-pressure emplacement of the Cycladic blueschist unit onto the Menderes nappes, Anatolide belt, western Turkey. *Journal of the Geological Society, London*, **158**, 769–780.

Gessner, K., Piazolo, S., Güngör, T., Ring, U., Kröner, A. & Passchier, C.W. 2001b. Tectonic significance of deformation patterns in granitoid rocks of the Menderes nappes, Anatolide belt, southwest Turkey. *International Journal of Earth Sciences*, **89**, 766–780.

Gessner, K., Ring, U., Johnson, C., Hetzel, R., Passchier, C.W. & Güngör, T. 2001c. An active bivergent rolling-hinge detachment system: the Central Menderes metamorphic core complex in western Turkey. *Geology*, **29**, 611–614.

Gessner, K., Collins, A.S., Ring, U. & Güngör, T. 2004. Structural and thermal history of poly-orogenic basement: U–Pb geochronology of granitoid rocks in the southern Menderes Massif, Western Turkey. *Journal of the Geological Society, London*, **161**, 93–101.

Giunchi, C., Kiratzi, A., Sabadini, R. & Louvari, E. 1996. A numerical model of the Hellenic subduction zone: active stress field and sea-level changes. *Geophysical Research Letters*, **23**, 2485–2488.

Glodny, J., Bingen, B., Austrheim, H., Molina, J.F. & Rusin, A. 2002. Precise eclogitisation ages deduced from Rb/Sr mineral systematics: the Maksyutov complex, Southern Urals, Russia. *Geochimica et Cosmochimica Acta*, **66**, 1221–1235.

Glodny, J., Ring, U., Kühn, A., Gleissner, P. & Franz, G. 2005. Crystallization and very rapid exhumation of the youngest Alpine eclogites (Tauern Window, Eastern Alps) from Rb/Sr mineral assemblage analysis. *Contributions to Mineralogy and Petrology*, **149**, 699-712, doi:10.1007/s00410-005-0676-5.

Godfriaux, I. 1968. Etude géologique de la région de l'Olympe (Grèce). *Annales Géologiques des Pays Helléniques*, **19**, 1–271.

Green, P.F., Duddy, I.R., Gleadow, A.J.W., Tinegate, P.R. & Laslett, G.M. 1986. Thermal annealing of fission tracks in apatite: 1. A qualitative description. *Chemical Geology*, **59**, 237–253.

Hurford, A.J. 1990. Standardisation of fission-track dating calibration: recommendation by the Fission Track Working Group of the IUGS Subcommission on Geochronology. *Chemical Geology*, **80**, 171–178.

Hurford, A.J. & Green, P.F. 1982. A user's guide to fission-track dating calibration. *Earth and Planetary Science Letters*, **59**, 343–354.

Inger, S. & Cliff, R.A. 1994. Timing of metamorphism in the Tauern Window, Eastern Alps: Rb–Sr ages and fabric formation. *Journal of Metamorphic Geology*, **12**, 695–707.

Jacobshagen, V. 1986. *Geologie von Griechenland*. Bornträger, Berlin.

Katsikatsos, G. 1991. *Geological Map of Greece, Rafina Sheet*. Institute of Geological Mining Research (IGME), Athens.

Katsikatsos, G., De Bruijn, H. & van der Meuler, A.J. 1981. The Neogene of the island of Euboea (Evia), a review. *Geologie en Mijnbouw*, **60**, 509–516.

Katzir, Y., Avigad, D., Matthews, A., Garfunkel, Z. & Evans, B.W. 2000.

Origin, HP/LT metamorphism and cooling of ophiolitic mélanges in southern Evia (NW Cyclades), Greece. *Journal of Metamorphic Geology*, **18**, 699–718.

Keay, S., Lister, G.S. & Buick, I.S. 2001. The timing of partial melting, Barrovian metamorphism and granite intrusion in the Naxos metamorphic core complex, Cyclades, Aegean Sea, Greece. *Tectonophysics*, **342**, 275–312.

Kiratzi, A. & Louvari, E. 2003. Focal mechanisms of shallow earthquakes in the Aegean Sea and the surrounding lands determined by waveform modeling: a new database. *Journal of Geodynamics*, **36**, 251–274.

Kissel, C., Laj, C. & Mazaud, A. 1986. First paleomagnetic results from Neogene formations in Evia, Skyros and the Volos region and the deformation of central Aegea. *Geophysical Research Letters*, **13**, 1446–1449.

Kokkalas, S. 2001. Tectonic evolution and stress field of the Kymi–Aliveri basin, Evia Island, Greece. *Bulletin of the Geological Society of Greece*, **34**, 243–249.

Kumerics, C., Ring, U., Brichau, S., Glodny, J. & Monié, P. 2005. The extensional Messaria shear zone and associated brittle detachment faults, Aegean Sea, Greece. *Journal of the Geological Society, London*, **162**, 701–721.

Lister, G.S., Banga, G. & Feenstra, A. 1984. Metamorphic core complexes of Cordilleran type in the Cyclades, Aegean Sea, Greece. *Geology*, **12**, 221–225.

Ludwig, K.R. 1999. *Isoplot/Ex Ver 2.06: a Geochronological Toolkit for Microsoft Excel*. Berkeley Geochronology Center Special Publications, **1a**.

Maluski, H., Vergely, P., Bavay, D., Bavay, P. & Katsikatos, G. 1981. $^{40}Ar/^{39}Ar$ dating of glaucophane and phengites in southern Euboa (Greece): geodynamic implications. *Bulletin de la Société Géologique de France*, **5**, 469–476.

Morris, A. 1995. Rotational deformation during Paleogene thrusting and basin closure in eastern central Greece—paleomagnetic evidence from Mesozoic carbonates. *Geophysical Journal International*, **121**, 827–847.

Müller, W., Dallmeyer, R.D., Neubauer, F. & Thöni, M. 1999. Deformation-induced resetting of Rb/Sr and $^{40}Ar/^{39}Ar$ mineral systems in a low-grade, polymetamorphic terrane (Eastern Alps, Austria). *Journal of the Geological Society, London*, **156**, 261–278.

Müller, W., Mancktelow, N.S. & Meier, M. 2000. Rb–Sr microchrons of synkinematic mica in mylonites: an example from the DAV fault of the Eastern Alps. *Earth and Planetary Science Letters*, **180**, 385–397.

Papanikolaou, D.J. 1978. Contribution to the geology of the Aegean Sea: the island of Andros. *Annales Géologiques des Pays Helléniques*, **29**, 477–553.

Pe-Piper, G. & Piper, D.J.W. 1994. Miocene magnesian andesites and dacites, Evia, Greece: adakites associated with subducting slab detachment and extension. *Lithos*, **31**, 125–140.

Richter, D., Mariolakos, I. & Risch, H. 1978. The main flysch stages of the Hellenides. *In:* Cloos, H., Roeder, D. & Schmidt, K. (eds) *Alps, Apennines, Hellenides*. Schweizerbart, Stuttgart, 434–438.

Ring, U. & Layer, P. W. 2003. High-pressure metamorphism in the Aegean, eastern Mediterranean: underplating and exhumation from the Late Cretaceous until the Miocene to Recent above the retreating Hellenic subduction zone. *Tectonics*, **22**, 1022, doi:10.1029/2001ITC001350.

Ring, U. & Reischmann, T. 2002. The weak and superfast Cretan detachment, Greece: exhumation at subduction rates in extruding wedges. *Journal of the Geological Society, London*, **159**, 225–228.

Ring, U., Gessner, K., Güngör, T. & Passchier, C.W. 1999a. The Menderes Massif of western Turkey and the Cycladic Massif in the Aegean—do they really correlate? *Journal of the Geological Society, London*, **156**, 3–6.

Ring, U., Brandon, M.T., Willett, S.D. & Lister, G.S. 1999b. Exhumation processes. *In:* Ring, U., Brandon, M.T., Lister, G.S. & Willett, S. (eds) *Exhumation Processes: Normal Faulting, Ductile Flow and Erosion*. Geological Society, London, Special Publications, **154**, 1–27.

Ring, U., Laws, S. & Bernet, M. 1999c. Structural analysis of a complex nappe sequence and late-orogenic basins from the Aegean Island of Samos, Greece. *Journal of Structural Geology*, **21**, 1575–1601.

Ring, U., Layer, P.W. & Reischmann, T. 2001. Miocene high-pressure metamorphism in the Cyclades and Crete, Aegean Sea, Greece: evidence for large-magnitude displacement on the Cretan detachment. *Geology*, **29**, 395–398.

Ring, U., Thomson, S.N. & Bröcker, M. 2003a. Fast extension but little exhumation: the Vari detachment in the Cyclades, Greece. *Geological Magazine*, **140**, 245–252.

Ring, U., Johnson, C., Hetzel, R. & Gessner, K. 2003b. Tectonic denudation of a Late Cretaceous–Tertiary collisional belt: regionally symmetric cooling patterns and their relation to extensional faults in the Anatolide belt of western Turkey. *Geological Magazine*, **140**, 421–441.

Ring, U., Will, T., Glodny, J., et al. 2007. Early exhumation of high-pressure rocks in extrusion wedges: the Cycladic blueschist unit in the eastern Aegean, Greece and Turkey. *Tectonics*, doi: 10.1029/2005TC001872.

Robertson, A.H.F., Clift, P., Degnan, P.J. & Jones, G. 1991. Palaeogeographic and palaeotectonic evolution of the Eastern Mediterranean Neotethys. *Palaeogeography, Palaeoclimatology, Palaeoecology*, **87**, 289–343.

Shaked, Y., Avigad, D. & Garfunkel, Z. 2000. Alpine high-pressure metamorphism at the Almyropotamos window (southern Evia, Greece). *Geological Magazine*, **137**, 367–380.

Stöckhert, B., Brix, M.R., Kleinschrodt, R., Hurford, A.J. & Wirth, R. 1999. Thermochronology and microstructures of quartz—a comparison with experimental flow laws and predictions on the temperature of the brittle–plastic transition. *Journal of Structural Geology*, **21**, 351–369.

Taymaz, T., Jackson, J. & McKenzie, D. 1991. Active tectonics of the north and central Aegean Sea. *Geophysical Journal International*, **106**, 433–490.

Thomson, S.N., Stöckhert, B. & Brix, M.A. 1998. Thermochronology of the high-pressure metamorphic rocks of Crete, Greece: implications for the speed of tectonic processes. *Geology*, **26**, 259–262.

Tomaschek, F., Kennedy, A., Villa, I.M. & Ballhaus, C. 2003. Zircons from Syros, Cyclades, Greece—recrystallization and mobilisation during high pressure metamorphism. *Journal of Petrology*, **44**, 1977–2002.

Tsokas, G.H. & Hansen, R.O. 1997. Study of the crustal thickness and the subducting lithosphere in Greece from gravity data. *Journal of Geophysical Research*, **102**, 20585–20597.

Vandenberg, L.C. & Lister, G.S. 1996. Structural analysis of basement tectonites from the Aegean metamorphic core complex of Ios, Cyclades, Greece. *Journal of Structural Geology*, **18**, 1437–1454.

van Hinsbergen, D.J.J., Zachariasse, W.J., Wortel, M.J.R. & Meulenkamp, J.E. 2005a. Underthrusting and exhumation: a comparison between the External Hellenides and the 'hot' Cycladic and 'cold' South Aegean core complexes (Greece). *Tectonics*, **24**, doi:10.1029/2004TC001692.

van Hinsbergen, D.J.J., Langereis, C.G. & Meulenkamp, J.E. 2005b. Revision of the timing, magnitude and distribution of Neogene rotations in the western Aegean region. *Tectonophysics*, **396**, 1–34.

Villa, I. 1998. Isotopic closure. *Terra Nova*, **10**, 42–47.

Wijbrans, J.R., Schliestedt, M. & York, D. 1990. Single grain argon laser probe dating of phengites from the blueschist to greenschist transition on Sifnos (Cyclades, Greece). *Contributions to Mineralogy and Petrology*, **104**, 582–593.

Xypolias, P., Kokkalas, S. & Skourlis, K. 2003. Upward extrusion and subsequent transpression as a possible mechanism for the exhumation of HP/LT rocks in Evia Island (Aegean Sea, Greece). *Journal of Geodynamics*, **35**, 303–332.

Received 28 March 2006; revised typescript accepted 4 August 2006.
Scientific editing by Tim Needham